

Validation of SMOS sea ice thickness retrieval in the northern Baltic Sea

By NINA MAAB^{1*}, LARS KALESCHKE¹, XIANGSHAN TIAN-KUNZE¹, MARKO MÄKYNEN², MATTHIAS DRUSCH³, THOMAS KRUMPEN⁴, STEFAN HENDRICKS⁴, MIKKO LENSU², JARI HAAPALA² and CHRISTIAN HAAS⁵, ¹*Institute of Oceanography, University of Hamburg, Hamburg, Germany*; ²*Finnish Meteorological Institute, Helsinki, Finland*; ³*European Space Agency, ESA-ESTEC, Noordwijk, The Netherlands*; ⁴*Alfred Wegener Institute Helmholtz Centre for Polar and Marine Research, Bremerhaven, Germany*; ⁵*Department of Earth and Space Science and Engineering, York University, Toronto, Canada*

(Manuscript received 14 April 2014; in final form 23 December 2014)

ABSTRACT

The Soil Moisture and Ocean Salinity (SMOS) mission observes brightness temperatures at a low microwave frequency of 1.4 GHz (L-band) with a daily coverage of the polar regions. L-band radiometry has been shown to provide information on the thickness of thin sea ice. Here, we apply a new emission model that has previously been used to investigate the impact of snow on thick Arctic sea ice. The model has not yet been used to retrieve ice thickness. In contrast to previous SMOS ice thickness retrievals, the new model allows us to include a snow layer in the brightness temperature simulations. Using ice thickness estimations from satellite thermal imagery, we simulate brightness temperatures during the ice growth season 2011 in the northern Baltic Sea. In both the simulations and the SMOS observations, brightness temperatures increase by more than 20 K, most likely due to an increase of ice thickness. Only if we include the snow in the model, the absolute values of the simulations and the observations agree well (mean deviations below 3.5 K). In a second comparison, we use high-resolution measurements of total ice thickness (sum of ice and snow thickness) from an electromagnetic (EM) sounding system to simulate brightness temperatures for 12 circular areas. While the SMOS observations and the simulations that use the EM modal ice thickness are highly correlated ($r^2=0.95$), the simulated brightness temperatures are on average 12 K higher than observed by SMOS. This would correspond to an 8-cm overestimation of the modal ice thickness by the SMOS retrieval. In contrast, if the simulations take into account the shape of the EM ice thickness distributions ($r^2=0.87$), the mean deviation between simulated and observed brightness temperatures is below 0.1 K.

Keywords: sea ice thickness, satellite remote sensing, Baltic Sea

1. Introduction

Changes in the polar sea ice cover are prominent indicators of climate change, and observing the Earth's sea ice volume is not only important for sea ice modelling, but also for navigational safety. While the sea ice area has been observed by satellites for several decades now, a continuous large-scale retrieval of sea ice thickness from space is still missing. Mainly three methods have been used to retrieve ice thickness from satellites in the past: (1) Altimeters measure the freeboard of sea ice, from which sea ice

thickness is inferred via Archimedes' principle (Laxon et al., 2003; Kwok and Rothrock, 2009). However, the relative error of altimeter-based ice thickness measurements is large for thin sea ice (Laxon et al., 2003). (2) The thickness of thin ice can be estimated from the ice surface temperature using thermal infrared imagery (e.g. Yu and Rothrock, 1996; Mäkynen et al., 2013). The major drawback of this temperature-based thickness retrieval is the requirement for cloud-free conditions, and thus, there may be long temporal gaps in the thickness chart coverage over a region of interest. In addition, discriminating clear-sky from clouds is difficult in winter night-time conditions (Frey et al., 2008). (3) There have been attempts to estimate ice thickness from passive microwave measurements at the

*Corresponding author.
email: nina.maass@uni-hamburg.de

19–90 GHz channels by exploiting the correlation between ice thickness and ice surface salinity (e.g. Martin et al., 2004; Naoki et al., 2008; Tamura and Ohshima, 2011). However, these techniques are restricted to ice thickness less than about 10–20 cm, and the quantification of thin ice thickness with 37 and 90 GHz data is not possible if the ice is covered by snow or a high area fraction of frost flowers (Hwang et al., 2007; Nihashi et al., 2009).

Since its launch in 2009, the Soil Moisture and Ocean Salinity (SMOS) mission has provided a complementary satellite-based technique for estimating sea ice thickness. SMOS brightness temperatures at 1.4 GHz have been used to retrieve sea ice thickness up to about 50 cm in the Arctic (Kaleschke et al., 2012; Huntemann et al., 2014; Tian-Kunze et al., 2014). For low-salinity ice, the retrieval is expected to be suitable also for thicker ice (Kaleschke et al., 2010). Here, we first investigate whether SMOS brightness temperatures in the northern Baltic Sea, which is characterised by low water and ice salinities, contain information on ice thickness (Section 4), and subsequently use airborne ice thickness measurements to investigate how the SMOS-retrieved ice thickness relates to the ice thickness distribution (Section 5).

The SMOS mission carries the first passive microwave radiometer that measures radiation in the L-band continuously from space. The SMOS measurements have a spatial resolution of about 35–50 km (depending on the incidence angle). The mission was originally designed to provide global estimates of SMOS. Since spring 2010, observations have been made available to scientific and operational users (Mecklenburg et al., 2012). The maximum ice thickness that can be retrieved from L-band radiometry depends on the dielectric properties of sea ice, which can be described by ice temperature and salinity (Kaleschke et al., 2010). For sea ice with a bulk temperature of $T_{ice} = -5^{\circ}\text{C}$ and a salinity of $S_{ice} = 8$ g/kg, which are typical values for 20–50 cm thick Arctic first-year ice (e.g. Cox and Weeks, 1983), the maximum retrievable ice thickness in L-band has been estimated to be about 50 cm, while it can be up to 1.5 m under less saline conditions of $S_{ice} < 1$ g/kg, typical for the Baltic Sea (Kaleschke et al., 2010). As the hitherto existing retrievals are based on bulk properties of the ice, they are technically only suitable for undeformed ice without pressure ridges.

The potential for the retrieval of sea ice thickness from L-band radiometry has been demonstrated with simultaneous airborne measurements of L-band brightness temperature and of ice thickness from electromagnetic (EM) induction measurements during the Pol-ICE campaign 2007 in the Baltic Sea (Kaleschke et al., 2010; Mills and Heygster, 2011). However, the results were difficult to interpret because (1) the campaign was conducted under wet snow conditions, which compromised the thickness

retrieval from L-band measurements, (2) the spatial overlap between the L-band and the EM measurements was relatively small, and (3) due to an unstable behaviour of the power converter the radiometer was not operating at its nominal performance (Kaleschke et al., 2010). Furthermore, results obtained for airborne radiometry are not necessarily transferable to satellite measurements, especially in a land-enclosed basin like the Baltic Sea (Fig. 1), where the land impact on SMOS measurements is relatively high and has mainly two implications. First, many of the observed brightness temperatures are influenced by land surfaces (land spill-over). At L-band frequencies, brightness temperatures over land and over ice are usually higher than over the open ocean. Thus, if footprints contain land surfaces, the resulting brightness temperatures may be erroneously allocated to the presence of ice, unless further processing of the data is applied (e.g. Maaß and Kaleschke, 2010). Second, we expect more man-made sources of L-band radiation (Oliva et al., 2012), that is, radio frequency interference (RFI), than in the Arctic. Both effects mainly restrict the availability of usable brightness temperature data. We expect that if the ice thickness retrieval with SMOS succeeds in a challenging region like the Baltic Sea,

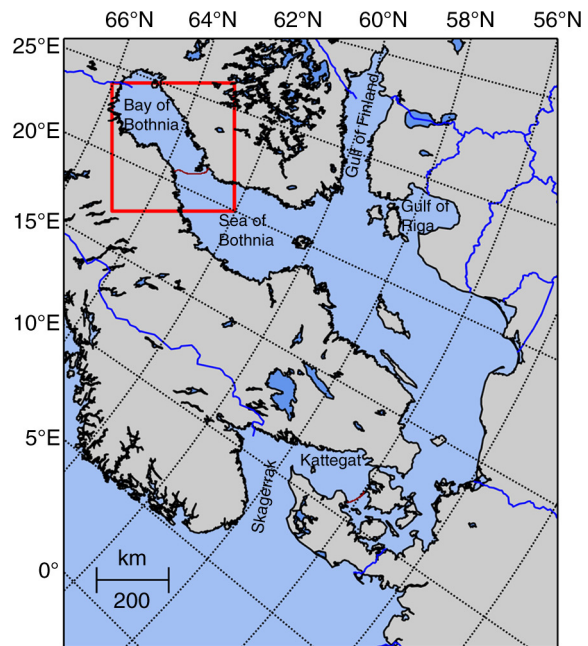


Fig. 1. The Baltic Sea area in polar stereographic projection with the projection plane at 70°N , as defined by the NSIDC (National Snow & Ice Data Center). The red box indicates the area in the Bay and Sea of Bothnia that is investigated in this study. The brownish line between the Bay and Sea of Bothnia indicates the approximate border between these areas, and the brownish line south of the Kattegat is the approximate border of the Baltic Sea, though the Kattegat is sometimes included as part of the Baltic Sea (Leppäranta and Myrberg, 2009).

it will probably also be applicable in other regions. Although the low-salinity conditions of the Baltic Sea are not representative for Arctic sea ice, a successful application of our emission model would suggest that, in principle, the model is able to describe the L-band brightness temperature of sea ice for given ice conditions, and thus may allow for the retrieval of ice thickness from SMOS measurements.

In previous studies, SMOS-retrieved ice thicknesses were compared to ice thickness maps obtained from MODerate resolution Imaging Spectroradiometer (MODIS) thermal infrared imagery, for example. The comparisons with up to 71 MODIS scenes from the winters 2009–2011 resulted in coefficients of determination r^2 between 0.36 and 0.5 (Kaleschke et al., 2012; Huntemann et al., 2014; Tian-Kunze et al., 2014). However, the uncertainty of ice thickness derived from MODIS is assumed to be 38–50% (Mäkynen et al., 2013). While these previous studies demonstrated that SMOS measurements contain information on thin ice thickness, they always assumed 100% ice concentration and did not account for snow on the ice. Snow has a two-fold impact on L-band brightness temperatures of sea ice (Maaß et al., 2013b): (1) Due to the snow’s thermal insulation, snow-covered ice is usually warmer than snow-free ice, and because the dielectric properties of ice depend on the ice temperature, snow thus influences the brightness temperature. (2) Additionally, snow causes the brightness temperature to be higher because the reflectivities between the air–snow and the snow–ice boundaries are lower than the reflectivity at the air–ice boundary. While some of the previous retrievals used semi-empirical approaches (Kaleschke et al., 2012; Tian-Kunze et al., 2014) that neglected the snow layer on the ice or included only the thermal insulation effect of snow (but not the radiometric effect), the retrieval in Huntemann et al. (2014) was based on a completely empirical approach, which did not allow for investigating the impact of the snow layer. In contrast, here we retrieve ice thickness with an emission model that includes a snow layer on the ice. This emission model has been used to study the impact of snow on L-band brightness temperatures in the Arctic (Maaß et al., 2013b). We use this new emission model to simulate brightness temperatures during the ice growth season in January and February 2011 in the northern part of the Baltic Sea (Section 4). Ice thickness in these model simulations is estimated using ice thickness maps from MODIS thermal infrared imagery produced by the Finnish Meteorological Institute (FMI). We compare these simulated brightness temperatures with SMOS observations and discuss the impact of the model assumptions for the presence of snow, the ice temperature, ice salinity and ice concentration. Additionally, we use our emission model to simulate brightness temperatures for ice thickness

distributions as observed during an airborne EM campaign in the northern Baltic Sea in March 2011 (Section 5). For these simulations, we also take into account the variable ice concentration. We discuss the information on ice thickness that is retrievable from SMOS data and compare different brightness temperature simulations with SMOS observations because being able to reproduce brightness temperatures as they are observed is an important part of the retrieval of ice parameters from SMOS measurements.

2. Sea ice emission model, data sets and methods

The study presented here is based on the following components: the sea ice emission model we use to simulate L-band brightness temperatures (Section 2.1); SMOS brightness temperature measurements (Section 2.2); our approach to retrieve ice thickness from SMOS data using the emission model (Section 2.3); ice thickness maps derived from thermal imagery and ice charts (Section 2.4); the SafeWin field campaign’s EM ice thickness measurements (Section 2.5); and ancillary data (Section 2.6).

2.1. Emission model

In this study, we use the emission model presented in Maaß et al. (2013b), which, in contrast to the previously used models for the SMOS ice thickness retrieval, accounts for a snow layer on top of the ice. Here we give only a short summary of the main features of the model, a more detailed description is found in Maaß et al. (2013b). The model is based on the emission model described in Burke et al. (1979), which is used to describe the radiation of a system that consists of one layer of snow that is on top of one layer of ice, under which is a semi-infinite (half-space) layer of sea water. The emission model calculates the brightness temperature as observed above the air–snow interface as a function of the temperatures and permittivities of snow, ice and water and of the thicknesses of the snow and the ice layers. In our model, the permittivities are calculated from empirical relationships. Namely, water permittivity mainly depends on water temperature and salinity (Klein and Swift, 1977); ice permittivity can be described as a function of brine volume fraction (Vant et al., 1978), which depends on ice salinity and the densities of the ice and the brine (Cox and Weeks, 1983), which in turn mainly depend on ice temperature (Pounder, 1965; Cox and Weeks, 1983); snow permittivity can be calculated from snow density, snow wetness and snow temperature (Tiuri et al., 1984). Here we consider only dry snow. A heat transfer equation is used to calculate the bulk temperatures of the snow and the ice layers from the ice surface temperature and the ice bottom temperature. The ice bottom temperature is assumed to be equal to the water temperature at freezing point.

Throughout this study, we use the notation ice surface temperature to refer to the temperature of the ice surface, which consists of snow for snow-covered ice and of ice for snow-free ice. Eventually, the input parameters for the model are ice and snow thickness, ice surface temperature, ice salinity, snow density, water temperature and water salinity. Additionally, the ice concentration is taken into account if the considered footprint area contains open water.

In this study, snow thickness (d_{snow}) is obtained through an empirical relationship based on ice thickness (d_{ice}), found for the Baltic Sea:

$$d_{snow} = 0 \text{ cm for } d_{ice} < 6 \text{ cm} \quad (1)$$

$$d_{snow} = 0.22d_{ice} - 1.3 \text{ cm for } d_{ice} \geq 6 \text{ cm} \quad (2)$$

This relationship is based on 172 ice and snow thickness measurements (< 50 cm) from Finnish ice breakers taken between 2006 and 2010 in the Baltic Sea; the standard error is 4.4 cm and the coefficient of correlation $r^2 = 0.21$ (Mäkynen, 2012).

2.2. SMOS data

SMOS is an Earth Explorer mission of the European Space Agency (ESA). The SMOS satellite was launched in November 2009. While it achieves a global coverage every 3 days, the polar regions and the Baltic Sea region are covered daily. The only payload of SMOS is a passive microwave 2-D-interferometric radiometer: the Microwave Imaging Radiometer using Aperture Synthesis (MIRAS). MIRAS measures the microwave radiation emitted from the Earth's surface at a frequency of 1.4 GHz in the L-band (Kerr et al., 2001). The corresponding wavelength is 21 cm. Every 1.2 seconds a 2-D snapshot is obtained, which contains observations under various viewing angles between 0 and 65°. The field of view is a hexagon-like shaped area about 1000 km across (Kerr et al., 2001). The spatial resolution is about 35 km for the lower incidence angles and about 50 km at the edge of the field of view (with higher incidence angles). MIRAS is a fully polarimetric radiometer; that is, it measures all four Stokes parameters. We use only the modified first and second Stokes parameters, that is, measurements at vertical and horizontal polarisation.

In this study, we use SMOS Level 1C Version 505 data. The Level 1C product contains multi-angular brightness temperatures at the top of the atmosphere. The data are geolocated in an equal-area Discrete Global Grid (DGG) system (Pinori et al., 2008) with a 15 km grid resolution. According to the information given in the SMOS data, the radiometric accuracy of a single measurement depends on its location within the snapshot (Tian-Kunze et al., 2014) and ranges between 3 and 7 K. In the Baltic Sea region,

SMOS provides on average about 120 measurements at different incidence angles per polarisation for each grid cell per day. Assuming that the variance decreases with $\frac{1}{\sqrt{N}}$, N being the number of single measurements, the radiometric accuracy of daily averages of 5° incidence angle bins, for example, would be about 1.0–2.3 K. For every SMOS grid point, we perform the data processing as described in Maaß et al. (2013b). This procedure includes a correction for geometrical rotation, Faraday rotation, and a filter for excluding brightness temperatures affected by RFI (Maaß et al., 2013b). The correction for geometrical and Faraday rotation is needed to calculate horizontally and vertically polarised brightness temperatures, while the correction is not needed for the brightness temperature intensity, which is the average between horizontal and vertical polarisation. Per snapshot, the MIRAS radiometer alternately measures one or two of the four Stokes vector components, of which all four are required for the transformation to horizontal and vertical polarisation. While in Maaß et al. (2013b) only subsequent snapshots are used for this procedure, here also data from the snapshot after the subsequent one is included. We apply a less restrictive criterion because, due to the relatively high RFI contamination, less data is available for the Baltic Sea region as compared to most Arctic regions.

In order to reduce land spill-over effects, we exclude all SMOS measurements with a land fraction of more than 6% within a square area of 40 km \times 40 km around the SMOS grid cell's centre point. The land–sea mask we use to determine the land fraction is the Global Self-consistent Hierarchical, High-resolution Shoreline Database (GSHHS) (Wessel and Smith, 1996).

2.3. SMOS ice thickness retrieval

The ice thicknesses we retrieve with SMOS in Section 5 are total ice thicknesses, that is, the sums of ice and snow thicknesses. In order to retrieve the total ice thickness, we apply our emission model to one ice and one snow layer. For dividing the total ice thickness into snow and ice thickness, as required by the model, we use eqs. (1) and (2). Additionally, the model is operated with information on ice concentration, ice temperature and salinity, water temperature and salinity, and snow density. For the retrieval, we use SMOS brightness temperatures at horizontal and at vertical polarisation with incidence angles θ between 0 and 65°.

To obtain the ice thickness, we perform three steps: First, we simulate brightness temperatures for a range of incidence angles ($\theta = 5, 12.5, 17.5, \dots, 62.5^\circ$) and a range of total ice thicknesses (here: 33–63 cm). In a second step, we collect all SMOS brightness temperatures and average the observations with $0^\circ \leq \theta < 10^\circ$, while the remaining observations are averaged over incidence angle bins of

5° (here: $10\text{--}15^\circ$, \dots , $60\text{--}65^\circ$). Finally, we calculate the root mean square deviations between the averaged SMOS brightness temperatures and the brightness temperatures that had been simulated for different total ice thicknesses in the first step. The ice thickness for which the root mean square deviation between the measured and the modelled brightness temperatures over the considered incidence angle range is lowest is the retrieved SMOS ice thickness.

2.4. MODIS-based ice thickness maps and ice charts

As ice thickness estimates in the Bay of Bothnia in Section 4, we use ice thicknesses retrieved from MODIS thermal imagery as produced by FMI (Mäkynen, 2012). In the retrieval, the surface heat balance equation is used to estimate ice thickness from ice surface temperature, which is obtained from MODIS measurements. The method works only for cloud-free and sufficiently cold weather conditions. The maps produced by FMI are cloud-masked by automatic and manual methods. The spatial resolution of the maps is 1 km. For Baltic conditions, the maximum retrievable ice thickness is about 40 cm for air temperatures below -20°C and reduces to about 15 cm for air temperatures between -10 and -5°C . The accuracy of the approach depends on the model parametrisations (e.g. for snow thickness) and assumptions (e.g. of linear temperature gradients) and the accuracy of the forcing data (e.g. for radiative and heat fluxes) (Mäkynen et al., 2013). Basically the method is only valid for level, thermodynamically grown ice. The uncertainty is estimated to be 40–50% for ice thicknesses between 20 and 50 cm and 26% for ice thicknesses between 10 and 15 cm. The MODIS-based ice thicknesses are consistent with ice thicknesses given in Finnish ice charts for the Baltic Sea (Mäkynen, 2012), which are manually produced by the Finnish Ice Service. For the daily ice chart production, ice analysts update previous charts using the available information from Synthetic Aperture Radar (SAR) images, drilling measurements near the coast, systematic field observations (including thickness) by the staff of icebreakers and other ships, and ice growth estimates obtained from ice models (Mäkynen, 2012).

In our investigations with an average ice surface temperature of $T_{surf} = -14.4^\circ\text{C}$ and ice thicknesses around 25–60 cm (Section 4), the uncertainty of the MODIS-derived ice thickness is about 40–50% and the maximum reliable ice thickness is expected to be 30–40 cm. However, in this study we also use higher MODIS-derived ice thicknesses up to 70 cm to roughly estimate the ice thickness for the brightness temperature simulations, because we found these ice thickness values to agree with Finnish ice charts.

2.5. EM ice thickness measurements during the SafeWin field campaign

In Section 5, we use ice thicknesses measured during the EU Safety of winter navigation in dynamic ice (SafeWin) project’s field campaign in the northern Baltic Sea. Between 2 and 7 March 2011, ice thickness in the Bay of Bothnia and the northern Sea of Bothnia was measured with a helicopter-towed EM Bird. The flight tracks of the 11 flights performed during the campaign are indicated in Fig. 2.

The EM Bird consists of a laser altimeter and an assembly of coils that transmit and receive low-frequency EM fields. While the transmitted and received EM fields allow for determining the sensor’s height above the conductive seawater surface, the laser altimeter measures the sensor’s altitude above the ice or snow surface. Over sea ice the difference between the sensor’s height above the ice surface and its height above the seawater corresponds to the total ice thickness, that is, the sum of ice and snow thickness (Haas et al., 2009). The EM Bird used in the SafeWin field campaign operates at a frequency of 4.06 kHz. The sampling frequency is 10 Hz, corresponding to a spacing of approximately 3–4 m between subsequent measurements. The laser altimeter has a higher sampling frequency of 100 Hz. The EM Bird is flown 10–20 m above the ice surface. The strength of the measured EM field represents the average field of an area approximately 3.7 times the instrument’s altitude above the ice surface; that is, the footprint is approximately between 37 and 74 m (Haas and Casey, 2012). The accuracy of EM ice thickness measurements over level ice is about 10 cm (Haas et al., 2009), whereas ice ridges can be underestimated by up to 50% (Haas and Jochmann, 2003). Therefore, sea ice thickness distributions obtained from EM measurements are most accurate with respect to their modal thickness (Haas et al., 2010). Because measuring ice thickness with the EM Bird is

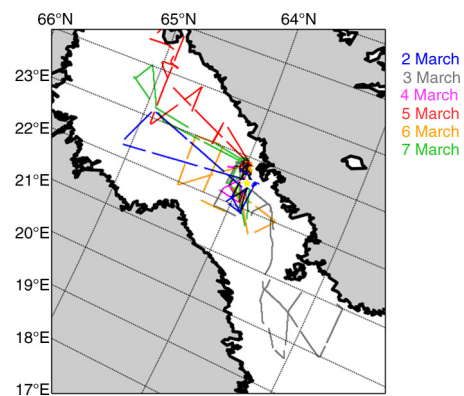


Fig. 2. Overview of all EM ice thickness flights performed in March 2011. The colours indicate the date of the flights. The yellow star indicates the approximate position of the ice salinity measurements.

only possible due to the higher conductivity of seawater compared to sea ice, the brackish nature of the Baltic Sea provides challenging conditions for EM ice thickness measurements. Additionally, the accuracy of EM ice thickness measurements in the Baltic Sea is further decreased in regions of shallow waters or freshwater layers under fast ice, that is, ice that is attached to shorelines or shoals (Haas, 2006).

2.6. Ancillary data

In Section 4, we use daily ice concentration data obtained from applying the ARTIST Sea Ice (ASI) algorithm (Kaleschke et al., 2001; Spreen et al., 2008) to Advanced Microwave Scanning Radiometer – Earth Observing System (AMSR-E) brightness temperature measurements at 89 GHz. These ice concentration maps have a grid spacing of 6.25 km. The ASI algorithm requires characteristic 89 GHz polarisation differences for open water and complete ice coverage. These tie points can vary regionally and temporally. Here we adapt the ice concentrations provided in the standard data set to Baltic Sea conditions by using Baltic Sea tie points that have been determined considering ice charts and high-resolution satellite images (Maaß and Kaleschke, 2010).

Compared to the 2-month analysis within a small area in Section 4, we consider a relatively short time period (2–7 March 2011) and a larger area in Section 5. For the area and time period considered in Section 5, several cloud-free MODIS images at 250 m resolution are available. The MODIS images taken over the Bay and Sea of Bothnia on the 3, 5, 6 and 8 March 2011 are cloud-free over large areas. For these images, the ASI ice concentration maps (even the ones adapted to Baltic Sea conditions) show lower ice concentrations than are visually inferable from the optical MODIS scenes. Thus, we decide to use the MODIS scenes instead of the more coarsely resolved (and land-impacted) ASI ice concentration maps for the brightness temperature simulations in Section 5. We produce ice concentration maps by applying a simple classification approach to the MODIS images at band 1 (wavelengths $\lambda = 620\text{--}670$ nm). All MODIS pixels with top of atmosphere reflectivities $r < 0.2$ are assigned to be open water pixels and all pixels with reflectivities $r \geq 0.2$ are assigned to be ice pixels.

In order to estimate the ice temperature in Sections 4 and 5, we use the MODIS ice surface temperature product MOD029. It is a daily product with a spatial resolution of 4 km and an estimated uncertainty of 1.2–1.3 K for cloud-free scenes (Hall et al., 2004).

As part of the SafeWin campaign, eight ice cores were taken between 28 February and 3 March 2011 within 20 km of approximately $63^\circ 56$ N, $22^\circ 22$ E (see Fig. 2), and the ice salinities of these samples were measured.

3. Baltic Sea ice

The Baltic Sea is a semi-enclosed brackish water basin of the Atlantic Ocean (Fig. 1) and is located in Northern Europe. The Baltic Sea has a surface area of about $400\,000$ km² and a mean depth of 54 m. The surface water salinity ranges from 25 g/kg in the Danish Straits (which connect the North and the Baltic Sea through the Skagerrak and the Kattegat), to 9 g/kg in the Southern Baltic Sea, to less than 1 g/kg in the innermost parts of the Gulf of Finland and the Bay of Bothnia, and to zero in river mouths (Leppäranta and Myrberg, 2009).

On average, the ice season in the Baltic Sea develops as following (Leppäranta and Myrberg, 2009): The ice cover begins to form in the middle of November, usually starting on the northern coast of the Bay of Bothnia and then progressing southward. The Bay of Bothnia freezes over in the middle of January, and about 1 month later the Sea of Bothnia, the Gulf of Finland and the Gulf of Riga are completely ice-covered as well. Melting starts in March, and in early May ice is only found in the Bay of Bothnia, where it melts completely by the end of May or beginning of June.

Both fast ice and drift ice are found in the Baltic Sea. The coastal archipelago areas are covered by fast ice, which forms a very stable ice cover. Even a thin land-fast sea ice cover is not broken up by wind and waves (Palosuo, 1963). In contrast, the drift ice further offshore shows a highly dynamic behaviour due to forcing by wind and currents. The motion of drift ice results in an uneven and broken ice field with distinct floes (several kilometers in size), leads and cracks, brash ice barriers, rafted ice and ice ridges. The upper limit for thermodynamically grown ice is 70 cm or less during most winters, the measured maximum being 120 cm (Palosuo et al., 1982). The thickness of ice ridges is typically 5–15 m and at maximum about 30 m (Leppäranta and Hakala, 1992).

Bulk salinity of Baltic Sea ice typically ranges between 0.2 and 2 g/kg (Hallikainen, 1992). Ice salinity data presented in Palosuo (1963) show that ice salinity can change rapidly; for example, in locations in the southern Sea of Bothnia the ice salinity had been observed to be almost 2 g/kg in mid-January and less than 0.7 g/kg at the beginning of March (Leppäranta and Myrberg, 2009). Although, in general, there is a North–South-gradient of ice salinity with lower ice salinities in the Bay of Bothnia than in the Sea of Bothnia, measurements indicate very different ice salinity profiles with bulk salinities in the Sea of Bothnia being partly higher, partly lower than in the Bay of Bothnia, as observed in land-fast sea ice (Granskog et al., 2006). Despite the low surface water salinities, ice formed in the Baltic Sea resembles sea ice formed in more saline oceans (Palosuo, 1961; Kawamura et al., 2001),

except for ice formed close to river estuaries with water salinities below 0.6 g/kg.

4. Temporal variability of simulated and observed brightness temperatures

In this section, we investigate whether our emission model is able to reasonably reproduce brightness temperatures as observed by SMOS over growing sea ice. Therefore, we compare our brightness temperature simulations with SMOS brightness temperatures measured between 1 January and 28 February 2011 in an almost completely ice-covered area located in the northern part of the Bay of Bothnia (Fig. 3).

4.1. SMOS observations

We consider SMOS brightness temperatures at horizontal and vertical polarisation at incidence angles θ between 0 and 65° that are located within the area indicated in Fig. 3. Figure 4 shows the temporal evolution of the brightness temperature intensity averaged over $\theta=0-40^\circ$; in this range the intensity is almost independent of θ . In order to investigate the effect of changing ice conditions, particularly of increasing ice thickness, on brightness temperatures, we divide the SMOS measurements into three different time

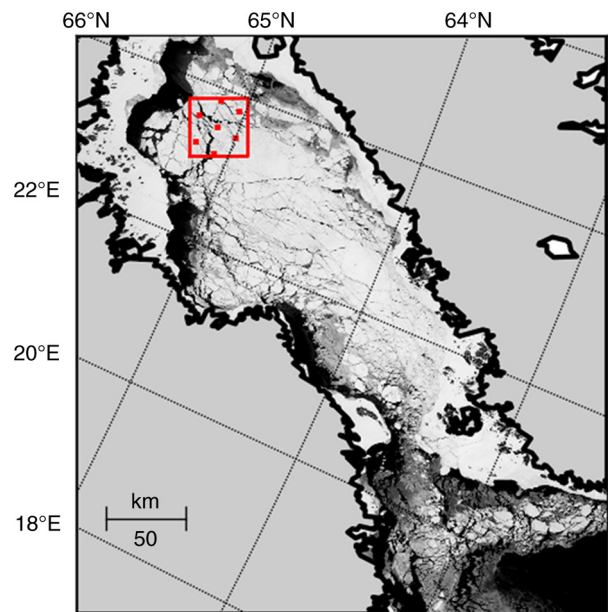


Fig. 3. MODIS image of Bay (and Sea) of Bothnia on 9 February 2011. The red square box (36 km \times 36 km) indicates the area selected for the comparison of simulated and SMOS-observed brightness temperatures from 1 January to 28 February 2011 (Section 4). The red points indicate the centre positions of SMOS measurements located within the box.

periods that contain approximately the same number of measurements: (1) 1–26 January, (2) 27 January–16 February and (3) 17–28 February. With the given partitioning, each time period contains between 3700 and 3900 individual SMOS measurements. The main reason why the three time periods have different lengths is that the availability of SMOS data is largely determined by RFI effects, which are temporally variable.

4.2. Model simulations

For simulating brightness temperatures with the emission model introduced in Section 2.1 and described in Maaß et al. (2013b), the following assumptions are made. The study area was almost completely ice-covered during the time period considered here, as indicated in Finnish ice charts, MODIS-based ice thickness maps, and ASI ice concentration data adapted to Baltic Sea conditions, which, for example, show a mean ice concentration of more than 98% within the investigated area (Fig. 4). Thus, we set the ice concentration in the emission model to $c_{ice} = 100\%$. For the model calculations, we assume a water salinity of $S_{water} = 3$ g/kg (Janssen et al., 1999). Water is assumed to be at the freezing point and thus at the corresponding temperature of $T_{water} = -0.2^\circ\text{C}$ (Fofonoff and Millard, 1983). The ice surface temperature T_{surf} for the model calculations is estimated from the MODIS ice surface temperature product MOD029 (Fig. 4). The corresponding average values are $T_{surf} = -13.5^\circ\text{C}$ for 1–26 January, $T_{surf} = -14.6^\circ\text{C}$ for 27 January–16 February, and $T_{surf} = -15.9^\circ\text{C}$ for 17–28 February. Although the ice surface temperature is quite variable and takes values between -25 and -5°C , we use average values for the three time periods. This is done for two reasons: (1) We do not have ice thickness information at the same temporal sampling rate, which is almost daily for T_{surf} , and thus, it would be difficult to interpret the resulting brightness temperature variations with regard to the impact of ice temperature as compared to ice thickness. (2) In our model, we assume a linear temperature gradient within the ice, which is not always a justified assumption for large temperature variations at the ice surface. For example, an assessment of the heat transfer in sea ice with representative values for Arctic sea ice suggests that a jump in the surface temperature from -10 to -30°C in 50 cm thick ice requires about half a day to re-establish a nearly linear temperature gradient within the ice column (Maaß, 2013). Thus, both (1) and (2) suggest that an average ice surface temperature is more suitable for our investigation of whether there is a signal from the ice thickness that can be observed with SMOS and of whether our emission model is able to reasonably reproduce the ice thickness evolution (and not the temperature variations).

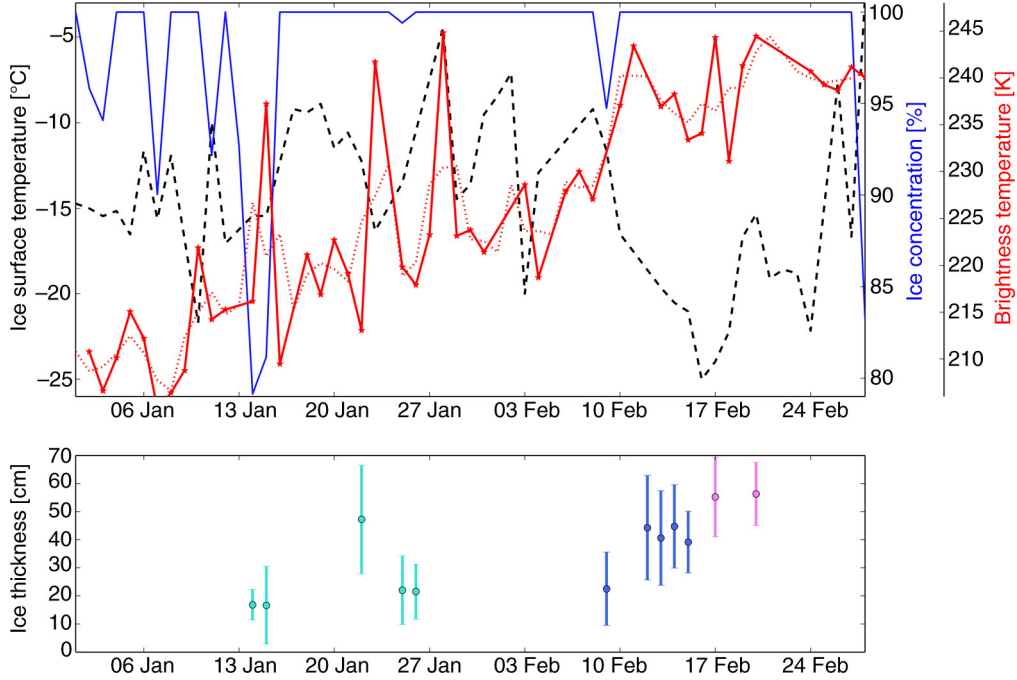


Fig. 4. Upper figure: Daily average of MODIS ice surface temperature MOD029 (dashed black), ASI ice concentration from AMSR-E with adaptation to Baltic Sea tie points (solid blue), and SMOS brightness temperature intensities (solid red) averaged over incidence angles from 0 to 40° for 1 January to 28 February 2011 for the investigated area in the Bay of Bothnia (see Fig. 3). Additionally, the 3-day-running mean of the SMOS brightness temperatures is shown (dotted red). Lower figure: Mean ice thickness (and standard deviation) in study area (50 km × 50 km) as obtained from the available MODIS ice thickness maps; the three colours indicate the three different time periods.

Regarding the ice salinity, we perform three different simulations with $S_{ice} = 0.5, 1.0, \text{ or } 1.5$ g/kg. We use our emission model with one snow and one ice layer and, for comparison, with one ice layer only. For the simulations that include snow, the snow thickness is estimated from eqs. (1) and (2). Model simulations in the Baltic Sea for the winters 1979–1990 show an average snow density of about 275 kg/m³ for January and February, which is somewhat higher than their value assumed for new snow ($\rho_{snow} = 225$ kg/m³), but considerably lower than their value assumed for water-soaked snow ($\rho_{snow} = 450$ kg/m³) in the Baltic Sea (Saloranta, 2000). We assume that $\rho_{snow} = 275$ kg/m³ is thus a realistic estimate for our brightness temperature simulations.

We use the MODIS ice thickness maps (Mäkynen, 2012) to estimate the ice thickness for the three selected time periods (Fig. 4). Because the spatial resolution of the MODIS ice thickness maps (1 km) is higher than that of the brightness temperature, ice surface temperature and ice concentration data sets and because the MODIS ice thickness maps are patchy due to the cloud masking, we use a slightly larger area (50 km × 50 km) for the MODIS ice thickness than for the other data sets (36 km × 36 km, see Fig. 3). For this area, five MODIS ice thickness maps are available for both the first and the second time period and two maps for the last time period, each with about 2000

pixels on average. For each map, we calculate the mean ice thickness and use the three average values of these mean ice thicknesses in our simulations: (1) $d_{ice} = 25 \pm 11$ cm (calculated from five values) for 1–26 January, (2) $d_{ice} = 38 \pm 8$ cm (calculated from five values) for 27 January–16 February and (3) $d_{ice} = 56 \text{ cm} \pm 1$ cm (calculated from two values) for 17–28 February. These values are in accordance with the ice thickness evolution as indicated in Finnish ice charts.

With the above assumptions for ice concentration, ice (and snow) thickness, ice salinity, surface temperature, snow density, and water temperature and salinity in our emission model, we simulate horizontally and vertically polarised L-band brightness temperatures for incidence angles between 0 and 65°.

4.3. Results

First, we calculate the root mean square deviations (Fig. 5) and mean differences (not shown) between the SMOS observations and the simulated brightness temperatures for the different simulation scenarios (regarding ice salinity and the presence or absence of a snow layer). For these comparisons, the brightness temperatures are averaged over incidence angle bins of 2.5°.

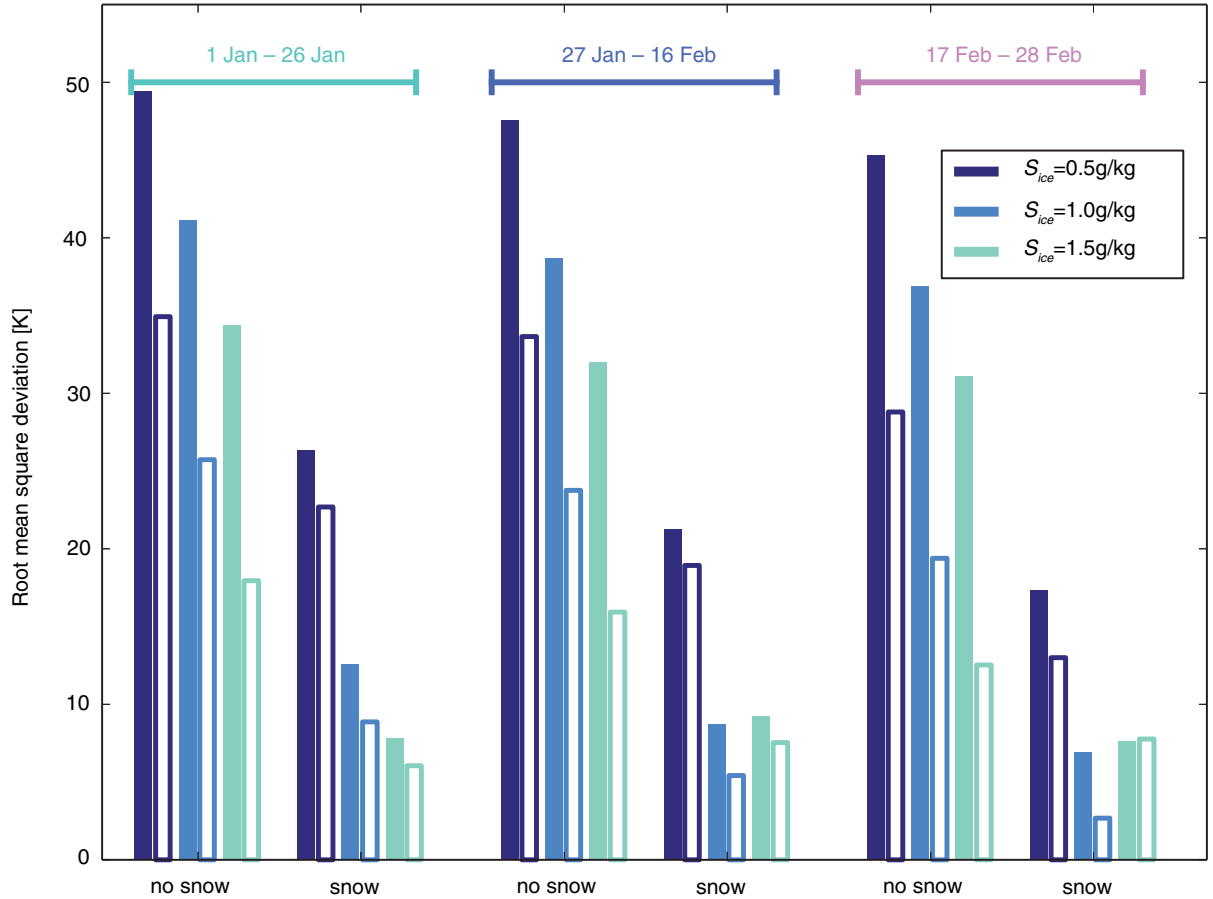


Fig. 5. Root mean square deviations between simulated and observed brightness temperatures averaged over all incidence angles. The time periods are indicated in the figure. The simulations are performed for ice without and with a snow cover (see annotation on the x-axis). The colour indicates the ice salinity assumed in the simulations (see legend). The filled bars indicate horizontal, the unfilled bars vertical polarisation.

The main results from the comparison are: (1) The root mean square and mean deviations between observed and simulated brightness temperatures are considerably larger if we do not include the snow layer. The average brightness temperatures modelled for snow-free ice conditions are at least (depending on the ice salinity assumption) 27–32 K lower than the observations at horizontal polarisation and 11–19 K lower at vertical polarisation (for the three time periods). This underestimation of observed brightness temperatures when neglecting the snow layer has also been found for Arctic sea ice (Maaß et al., 2013b). (2) The deviations between observations and simulations are generally smaller at vertical than at horizontal polarisation. (3) The root mean square deviations decrease with time, that is, from the first period with the lowest estimated ice thickness to the third period with the highest estimated ice thickness. (4) The simulated brightness temperatures are relatively sensitive to ice salinity at these low ice salinity values. (5) The lowest root mean square deviations for the

three time periods are obtained when snow is taken into account and the ice salinity is set to $S_{ice} = 1.5$ g/kg for the first time period (1–26 January), and to $S_{ice} = 1.0$ g/kg for the remaining time (27 January–16 February and 17–28 February). For these ice salinity assumptions in the model, the root mean square deviations between the simulations and the observations for the three time periods are between 6.9 and 8.7 K at horizontal and between 2.7 and 6.1 K at vertical polarisation. In Fig. 6, the simulations for these ice assumptions (i.e. snow included and using the above given ice salinities) are compared to the observed brightness temperatures as a function of incidence angle.

We do not show here that we also found that due to the high variability of SMOS measurements, the deviations are higher when we compare our simulations to single SMOS measurements instead of to SMOS measurements averaged over 2.5° incidence angle bins. The high variability of individual SMOS measurements is also visible in Fig. 6. However, most of the SMOS measurements are within the range

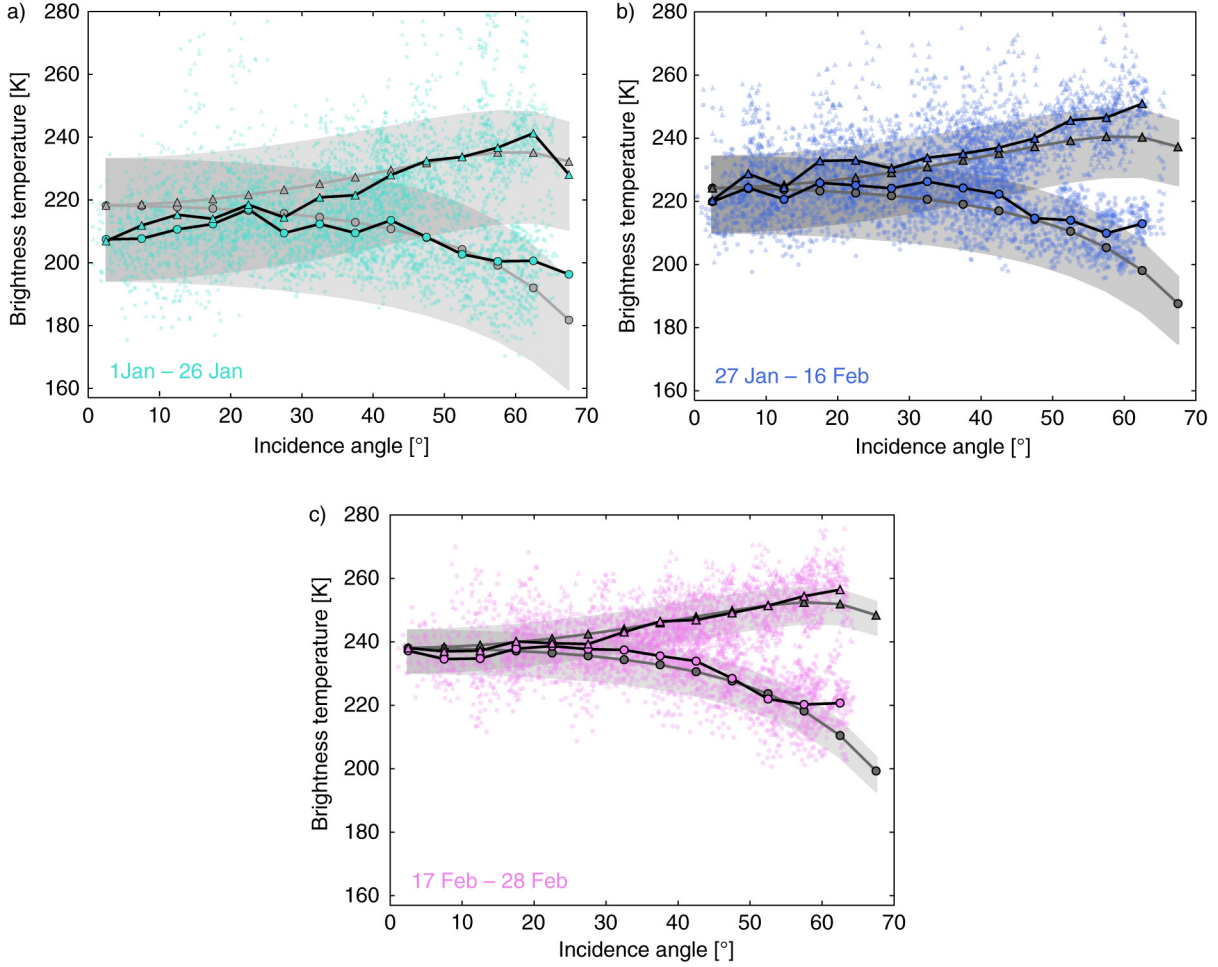


Fig. 6. Comparison of simulated (grey) and mean observed SMOS brightness temperatures (black). The uppermost figure shows the results for 1–26 January and a mean ice thickness of $d_{ice} = 25$ cm, the middle figure for 27 January–16 February and $d_{ice} = 38$ cm, and the lowest figure for 17–28 February and $d_{ice} = 56$ cm. Grey shaded areas indicate the model’s range of brightness temperatures for ice thicknesses ± 10 cm around the average value. Circles indicate horizontal polarisation, triangles vertical polarisation. The small coloured circles and triangles indicate individual SMOS measurements.

of brightness temperatures modelled for an ice thickness range of ± 10 cm around the assumed mean ice thickness. The incidence angle dependencies of the averaged observed and the simulated brightness temperatures are similar (Fig. 6). On average, the SMOS brightness temperatures of the three time periods clearly increase with time (Figs. 4 and 6). When averaging the 2.5° incidence angle bin mean values over the whole incidence angle range, the horizontally polarised SMOS brightness temperature increases from 208 ± 6 K to 220 ± 5 K and finally to 232 ± 7 K for the three subsequent time periods. At vertical polarisation, the average SMOS brightness temperature increases from 223 ± 10 K to 235 ± 8 K and finally to 245 ± 6 K. For the three time periods and both polarisations, the average deviations between the simulations and the observations are between -3.5 and $+3.4$ K. These deviations are lower

than the standard deviations of the SMOS observations and considerably lower than the observed increase in brightness temperature.

4.4. Sensitivity of brightness temperature to different ice parameters

For our brightness temperature simulations, we assumed certain values for the ice parameters (e.g. ice salinity) in the emission model. These assumptions contain uncertainties, and we try to estimate the resulting uncertainty for the modelled brightness temperature (Table 1). This is done by assuming constant average values for all model parameters except for one. This one parameter is varied within a range of values, which is determined by the estimated uncertainty of the considered parameter. This approach provides

Table 1. The ice parameters that influence the simulated brightness temperature, their mean value: $\langle r \rangle$ (as used in the simulations for all parameters except for the one that is varied), the range by which the parameter r is varied: Δr (if not specified, the parameter takes values between $\pm 0.5\Delta r$ around $\langle r \rangle$, otherwise the range is given in parentheses), and the resulting impact on the nadir brightness temperature intensity: ΔTB

	January/February 2011			March 2011		
	$\langle r \rangle$	Δr	ΔTB [K]	$\langle r \rangle$	Δr	ΔTB [K]
d_{ice}	40 cm	35 cm (25–60 cm)	37.2	40 cm	30 cm (30–60 cm)	21.3
T_{surf}	-15°C	10 K	17.0	-3.7°C	2 K	10.1
S_{ice}	1.0 g/kg	0.5 g/kg	12.4	0.5 g/kg	0.2 g/kg	8.8
d_{snow}	8 cm	6 cm	6.8	8 cm	6 cm	3.4
ρ_{snow}	275 kg/m ³	100 kg/m ³	1.3	310 kg/m ³	100 kg/m ³	1.0
c_{ice}	100%	3% (97–100%)	3.9	95%	4%	5.8
T_{water}	-0.2°C	0.15 K (-0.25 to -0.10°C)	0.9	-0.2°C	0.15 K (-0.30 to -0.15°C)	2.7
S_{water}	3 g/kg	2 g/kg	0.0	4 g/kg	2 g/kg	0.0
Σ			22.5			15.3

Σ is the (root mean square) sum of the impacts of all parameters except the ice thickness on the simulated brightness temperature.

a simple mean to estimate and to compare the different model parameters' impact on brightness temperature. By comparing the brightness temperature's sensitivity to these parameters with the sensitivity to ice thickness, we can also estimate the expected uncertainty of the SMOS ice thickness retrieval.

Table 1 gives the average values of the ice parameters used for the sensitivity analysis (as encountered during the examined time period), the estimated range of values they may take, and the resulting impact on the brightness temperature intensity (at nadir view, i.e. $\theta = 0^{\circ}$). The range of values for the ice surface temperature is assumed to be -20 to -10°C because the temperature was mostly between these values, although it was actually even more variable during the examined time period (Fig. 4). However, as the uncertainty of the MODIS ice surface temperature product is given to be 1.2–1.3 K (Hall et al., 2004) and average brightness temperatures (and ice surface temperatures) are considered here, an estimated range of 10 K is quite large and average values over several days may be expected to have smaller uncertainties. Uncertainty in snow density has been estimated to be 50 kg/m³ over first-year ice (Alexandrov et al., 2010), which we use as a rough estimation also for Baltic Sea ice. As the best results in the above comparison of SMOS observations and simulations were found for ice salinities of 1.5 and 1.0 g/kg, we assume an ice salinity range of 0.5 g/kg. For the snow thickness, we use the range of values proposed by the empirical relationship, given by eqs. (1) and (2), for the considered ice thicknesses of 25–60 cm, i.e. $d_{\text{snow}} = 5$ –11 cm. The mean ice concentration is assumed to range between 97 and 100% because the average values for the three time periods are within this range. The water salinity is assumed to be 3 ± 1 g/kg, and the water temperature within the corresponding range of freezing temperatures of water, that is, -0.25 to -0.1°C .

Compared to the other ice parameters, the increasing ice thickness has the highest impact on the brightness temperature. The impact by the increasing ice thickness ($\Delta TB = 37.2$ K) is even higher than the overall impact by all other parameters ($\Delta TB = 22.5$ K, calculated using Gaussian error propagation). For these conditions, the assumptions for the ice parameters and their estimated uncertainties would lead to an uncertainty of the ice thickness retrieval of about 11 cm. It would be about 7 cm if the uncertainty of the surface temperature was assumed to have the value given in the MODIS product (1.3 K), which would probably be an appropriate estimate for the average T_{surf} values.

4.5. Discussion

We hypothesise that the brightness temperature increase observed over the examined time period of 1 January to 28 February 2011 is related to the ice thickness, which increased by around 31 cm according to the MODIS ice thickness maps. However, altogether four of the input parameters of our emission model have the potential to cause a gradual brightness temperature increase of more than 20 K as observed in this case: (1) ice temperature, (2) ice salinity, (3) ice concentration and (4) ice thickness. In contrast, the model input parameters snow density, water temperature and water salinity do not have a large impact on the brightness temperature (Table 1), as long as the assumptions are within a realistic range of values. Regarding the impact of snow, there are two different aspects to consider: the presence of snow and the thickness of the snow cover. The brightness temperature's dependence on the thickness of the snow cover originates from the thermal insulation effect of snow. Snow-covered ice is usually warmer than bare sea ice, the thicker the snow cover the more the ice is insulated, and because the ice permittivity

depends on the ice temperature, snow has an (indirect) influence on brightness temperature (Maaß et al., 2013b). However, as long as the brightness temperature is not saturated with respect to ice thickness, brightness temperature does increase with snow thickness but the sensitivity to snow thickness is small compared to the sensitivity to ice thickness [Maaß et al. (2013b) and Table 1]. In contrast, the presence of snow has a large impact on the modelled brightness temperatures. The reason is that the reflectivities at the air–snow and at the snow–ice interfaces differ from the reflectivity at an interface between air and ice [as observed for a frequency of 6.7 GHz in Barber et al. (1998); Perovich et al. (1998) and as discussed for 1.4 GHz in Maaß et al. (2013b)]. As a consequence, according to our emission model, the emergence of snow would appear as a sudden increase of brightness temperature instead of a gradual increase of brightness temperature over 2 months. Thus, we exclude snow as the main cause for the observed brightness temperature increase. The possible contributions of the remaining four ice properties are discussed in the following:

- (1) **Ice temperature:** According to MODIS data, the snow surface temperature T_{surf} was always well below -5°C during the examined time period (Fig. 4). Sensitivity studies have suggested that for $T_{surf} < -5^{\circ}\text{C}$, brightness temperatures increase with increasing ice surface temperature (Maaß, 2013). However, the ice surface temperature data (Fig. 4) show rather irregular fluctuations with frequent changes between warming and cooling of the ice surface with a slight decrease of the mean ice surface temperature from -13.5°C (1–26 January) to -15.9°C (17–28 February). Consequently, the brightness temperature increase with time cannot be explained by changes in ice temperature, even less by a slightly decreasing ice temperature.
- (2) **Ice salinity:** We assume that the ice salinity in the northern Bay of Bothnia is less than 2 g/kg, and due to desalination processes that occur in growing or aging sea ice, we expect ice salinity generally to decrease with time. Sensitivity studies have suggested that brightness temperatures decrease with decreasing ice salinity if all other parameters are kept constant and ice salinities are below 2 g/kg (Maaß, 2013). Hence, ice salinity is not likely to have caused the increase of brightness temperatures observed here.
- (3) **Ice concentration:** According to Finnish ice charts, MODIS-based ice thickness maps, and ASI ice concentration data, the investigated area was almost completely ice-covered during the whole time period considered here (Fig. 4). According to the ASI ice concentration time series, the average ice concentration slightly increased from 97.2 to 99.7% from the first to the second time period. According to our sensitivity analysis (Table 1), the corresponding expected increase in brightness temperature would be an order of magnitude smaller than the observed increase. Thus, we are confident that the observed brightness temperature increase was not related to changes in the ice concentration.
- (4) **Ice thickness:** Finnish ice charts show that the ice thickness gradually increases from the beginning of January to the end of February 2011. Although the maximum reliable ice thickness that is retrievable from MODIS images is given to be about 40 cm (Mäkynen, 2012), we used the MODIS ice thickness maps to estimate ice thickness up to 70 cm. However, even if the absolute values are rather tentative estimates, they provide a strong indication that there was an increasing trend in ice thickness, and the ice thickness was most likely the main contributor to the observed brightness temperature increase with time.

As an additional indicator, we may consider the correlations between the observed brightness temperatures and the time series for ice thickness, ice concentration and ice surface temperature. In agreement with the above findings, the coefficient of determination between the 3-day running mean values of the SMOS brightness temperature and the MODIS ice thicknesses is higher ($r^2=0.57$ for the $n=12$ mean values from the MODIS maps) than the ones between the SMOS observations and the ASI ice concentration ($r^2=0.10$ for $n=12$; $r^2=0.01$ for the whole time period) or the MODIS ice surface temperature ($r^2=0.35$ for $n=12$; $r^2=0.05$ for the whole time period).

The Baltic Sea is a challenging area for the ice thickness retrieval with SMOS. L-band measurements in the Baltic Sea region suffer from a quite high RFI contamination, and the land impact on measured brightness temperatures is high in the land-enclosed Baltic Sea basin. We tried to filter out the effects of both disturbing sources by excluding measurements (1) with too high brightness temperatures (RFI filter), or (2) with inconsistent brightness temperatures with regard to their dependence on incidence angle (RFI filter), or (3) located too close to the coast. However, we expect RFI and the land spill-over still to be uncertainty sources. Furthermore, we found that RFI contamination in the Baltic Sea was temporally very variable and led to an exclusion of about 5–80% of the daily data in January and February 2011. ESA has made an effort of getting RFI sources switched off (Oliva et al., 2012), thus, it can be expected that the fraction of SMOS measurements affected by RFI has decreased since the beginning of 2011, and the

conditions for retrieving ice thickness from SMOS data in the Baltic Sea have improved.

The highest uncertainty in the above presented results is probably related to the ice salinity. First, the available information on ice salinity is usually restricted to individual measurements and/or model simulations. Second, the sensitivity of brightness temperature to ice salinity is very high for very low ice salinities [see Table 1 and Maaß (2013)]. Compared to the average bulk ice salinity of 0.5 g/kg obtained from the ice salinity measurements made between 28 February and 3 March 2011 during the SafeWin campaign in an area farther south (Section 2.6), the values that agree best (1.5 and 1.0 g/kg, respectively) may appear to be quite high. Thus, eventually we cannot distinguish whether (1) the emission model is slightly biased, for example, regarding the calculation of the ice temperature as suggested by Maaß et al. (2015), such that we obtain the best agreement with SMOS observations for slightly too high ice salinity assumptions in the model, or (2) the ice salinity assumptions are realistic and reflect the natural spatial and temporal variability of ice salinity in the Baltic Sea (see also Section 3), or (3) the MODIS-based retrieval is slightly underestimating ice thickness, such that with the too small ice thickness values in the emission model too high ice salinities result in a better agreement with SMOS observations. In general, we can state that although SMOS brightness temperatures in the Baltic Sea, according to our results here, can be used to infer information on the relative change in ice thickness, the uncertainty of the absolute ice thickness values caused by the uncertainty of the ice salinity assumption can be quite high. If we assumed that all other ice parameters were known exactly, the ice thickness uncertainty would be about 6 cm for an ice salinity uncertainty of 0.25 g/kg and about 12 cm for an uncertainty of 0.5 g/kg (for the ice conditions as defined by the average values in Table 1 for January/February 2011). The necessity to know the ice salinity may be avoided, if a retrieval that is (partly) based on SMOS data itself was used, for example, by using brightness temperature tie points for very thin ice and for the maximum retrievable ice thickness. However, on the other hand, the brightness temperature's high sensitivity to ice salinity may provide an opportunity to infer information on the ice salinity if information on the ice thickness and the other ice parameters is available.

5. Spatial variability of simulated and observed brightness temperatures and ice thickness

In this section, we approach the question how the ice thickness information contained in SMOS brightness temperatures may be interpreted. We use the high-resolution

ice thickness data obtained from EM measurements during the SafeWin campaign (2–7 March 2011) and the resulting ice thickness distributions to simulate brightness temperatures. Besides comparing these simulations with SMOS observations, we compare the EM ice thickness measurements with the ice thickness we would retrieve from SMOS data using the approach described in Section 2.3. Due to the EM measurement principle, ice thickness within this section is always total ice thickness, that is, the sum of ice and snow thickness.

5.1. Comparing SMOS and EM data

Comparing measurements obtained from EM sounding and from the SMOS satellite is challenging because every SMOS measurement represents an area of about 35–50 km diameter (depending on incidence angle), while single EM measurements have footprints on the order of 50 m length. In addition, SMOS measurements are located on a regular grid, while the EM measurements are distributed irregularly. We choose to divide the area covered by the SafeWin campaign's flight tracks into 12 circular areas of different sizes (Fig. 7) and assume that the ice thickness distribution within each of these circles is reasonably represented by the EM measurements (Fig. 8). The circles 1–8 contain between about 60000 and 185000 individual EM measurements, while the circles 9–12 contain between about 11000 and 22000 measurements. The selection of the circles is further explained and discussed in Section 5.5.

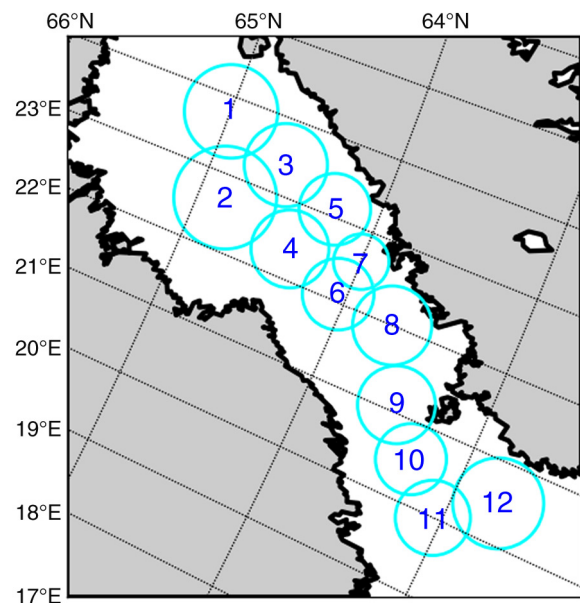


Fig. 7. Numbers of the 12 circles used for the comparison of EM and SMOS measurements. The diameters of the circles range from 36 to 66 km.

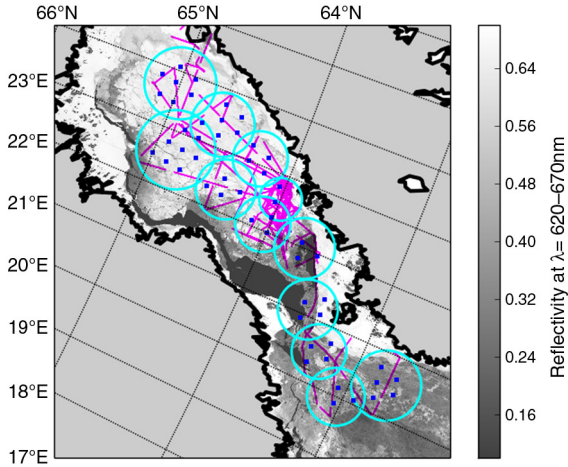


Fig. 8. Distribution of EM and SMOS measurements in the Bay and Sea of Bothnia and the 12 circular areas chosen for comparison of ice thicknesses. Pink lines indicate EM flight tracks, blue dots show the positions of SMOS measurements. These are overlaid on a MODIS image showing the reflectivities in band 1 (wavelength $\lambda = 620\text{--}670\text{ nm}$) on 3 March 2011.

For each circle, we include all SMOS measurements whose centre points are located within the inner 66% of the circle (Fig. 8). This restriction is chosen quite arbitrarily and is a compromise between including as many measurements as possible and excluding SMOS measurements that have contributions from large areas outside the circle. The EM flight tracks located within circles 9 and 12 are single lines through the circles rather than covering representatively the defined circular areas. Thus, for circle 9 we exclude the SMOS measurements located north of 63.6°N , and for circle 12 we exclude the SMOS measurements located south of 62.65°N .

In order to determine a suitable bin width for the comparison of EM-measured and SMOS-retrieved ice thicknesses for the 12 circles, we use Doane’s formula (Doane, 1979). It suggests the number of bins for the comparison of n values (here: $n = 12$) from a distribution with a known skewness (here: the average skewness of the 12 ice thickness distributions). According to the formula, the comparison should be done for five bins, which in our case means that we consider five ice thickness classes. Because the retrieval (as described below) gives values between about 33 and 63 cm, we consider the ice thickness classes (1) 33–39 cm, (2) 39–45 cm, (3) 45–51 cm, (4) 51–57 cm and (5) 57–63 cm. The bin width of 6 cm is also used to illustrate the EM ice thickness distributions.

5.2. Model simulations

Using our emission model, we simulate brightness temperatures at horizontal and at vertical polarisation for incidence

angles between 0° and 65° . These are compared with observed brightness temperatures and used to retrieve ice thickness. For the retrieval, brightness temperatures are simulated for the five average values of the ice thickness classes mentioned above, that is, for $d_{total} = 36, 42, 48, 54$ and 60 cm . For the comparison with observations, brightness temperatures are simulated for the modal and mean EM ice thicknesses, as well as the EM ice thickness distributions. The brightness temperature Tb for the ice thickness distribution is simply assumed to be the average brightness temperature for the encountered ice thicknesses taking into account their fractional occurrence within each circle:

$$Tb = \sum_i \frac{n(d_{ice,i})}{N} Tb_{sim}(d_{ice,i}), \quad (3)$$

where $n(d_{ice,i})$ is the number of EM measurements with ice thickness $d_{ice,i}$, N is the total number of EM measurements, and $Tb_{sim}(d_{ice,i})$ is the brightness temperature simulated for an ice thickness $d_{ice,i}$. In the emission model, we consider one ice layer that is covered by one layer of snow. First, we thus account for the impact of a snow cover on the brightness temperatures [change of ice permittivity due to thermal insulation by snow + change of reflectivities due to presence of snow (Maaß et al., 2013b), see also results of Section 4]. Second, the ice thickness measured by the EM Bird is total ice thickness (ice + snow thickness). In the emission model, the following assumptions are made for the (1) ice concentration, (2) ice temperature, (3) ice salinity, (4) water salinity, (5) water temperature and (6) snow thickness and density:

- (1) Ice concentration: As reasoned in Section 2.6, we use the largely cloud-free MODIS scenes in the Bay and Sea of Bothnia on the 3, 5, 6 and 8 March 2011 and determine for each 250 m grid box whether it represents water or ice. After having classified each available MODIS image, we average over all available days. The resulting field then contains values between 0 and 100% ice coverage (Fig. 9). In the emission model, we use a spatially weighted average value from this time-averaged ice concentration field for each of the 12 circular areas. These 12 ice concentration values are determined by including all MODIS pixels within the inner 66% of the validation circle with radius R_i ($i = 1, \dots, 12$) – the criterion for including SMOS pixels – plus 25 km outwards – the maximum distance of areas contributing to a SMOS measurement according to the SMOS footprint size of up to $50\text{ km} \times 50\text{ km}$. The included MODIS pixels are then weighted using the SMOS footprint’s mean weighting function (independent of incidence angle) (CESBIO, 2007) such

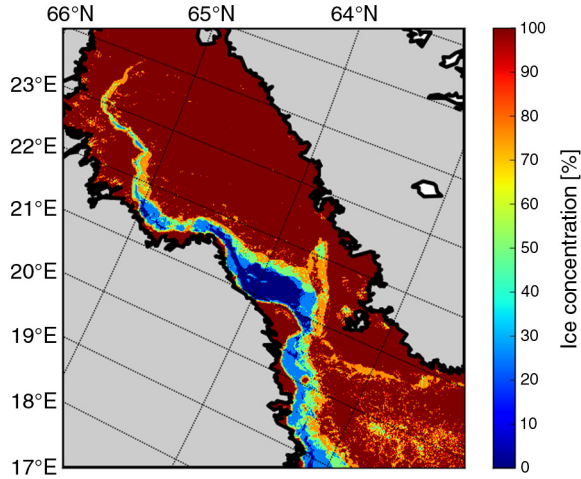


Fig. 9. Mean ice concentration for 2–7 March 2011 obtained from averaging classified MODIS images from 3, 5, 6 and 8 March. In the classification, each MODIS pixel (resolution 250 m) is determined to be covered either by water or ice (Section 2.6).

that the pixels in an inner radius of $R = 0.66R_i - 5$ km are equally weighted, and the weighting of the pixels outside of this inner circle decreases with distance as specified by the SMOS footprint’s weighting function. The resulting mean ice concentration values, which are used in the emission model, range between 66 and 100% and are given in Fig. 13. Within three circles (8, 10 and 11), the ice concentration varied by more than 10% during 2–7 March (Fig. 10). Furthermore, the MODIS images (not shown here) reveal that within circle 12 a lead in the ice opened up, although this is not reflected by the ice

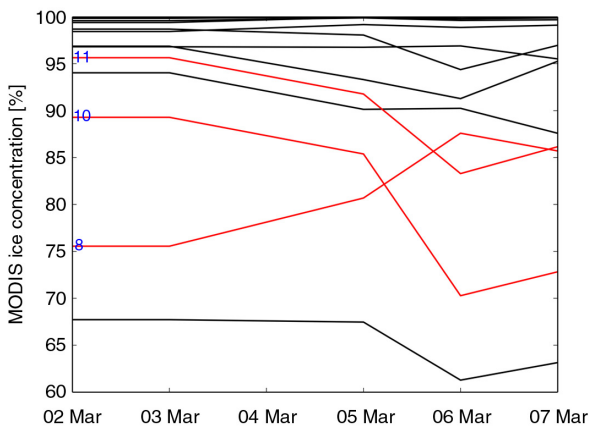


Fig. 10. Ice concentration as determined from classifying MODIS images from 3, 5, 6 and 8 March 2011 (Section 2.6) for the 12 circular areas. The ice concentration maps were interpolated to the time period of the SafeWin campaign (2–7 March 2011). The circles 8, 10 and 11, in which the ice concentration during the campaign varied by more than 10%, are shown in red.

concentration evolution where the ice concentration did not decrease by more than 10%.

- (2) Ice surface temperature: As in Section 4, we use the MOD029 ice surface temperature product (Hall et al., 2004). For determining 12 values to use in the emission model, we apply the same temporal and spatial averaging procedure as described above for the ice concentration. The resulting ice surface temperatures range between -4.9 and -2.9°C (see Fig. 13). Temperatures within the southerly circles are between -6 and -4°C on 2 March, all temperatures increase to about -3 to -1°C on 3–4 March and decrease again during 5–7 March with a North–South temperature gradient of about 4 K (Fig. 11).
- (3) Ice salinity: According to Finnish ice charts, the campaign area had been covered by ice for 1–2 months, and the modal ice thicknesses measured during the flight campaign were mainly between 30 and 60 cm. Thus, we expect desalination to have taken place in the ice and suppose $S_{ice} = 0.5$ g/kg to be a reasonable assumption for our simulations. This is supported by the ice salinity measurements carried out during the SafeWin campaign, which resulted in an average bulk ice salinity of 0.5 ± 0.1 g/kg. This value is also in agreement with the evolution of ice salinity according to measurements made in 1960 in Mäskär (approximately at 63.8°N , 22.6°E), where the bulk ice salinity decreases from about 0.8 g/kg at the end of January to about 0.5 g/kg throughout March (Leppäranta and Myrberg, 2009). Compared to the ice salinity values for that the

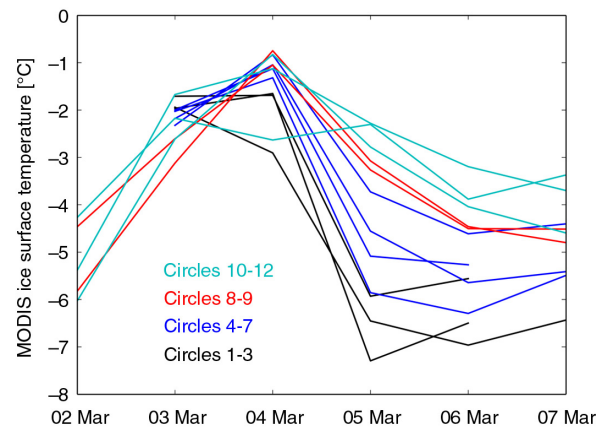


Fig. 11. MODIS ice surface temperature during the SafeWin campaign (2–7 March 2011) for the 12 circular areas depicted in Fig. 7. The curves are sorted by colours, as given in the figure, from the northernmost circles (black, circles 1–3) to the southernmost circles (cyan, circles 10–12).

simulations agreed best with the observations in the northern Bay of Bothnia in Section 4 (1.5 g/kg for 1–26 January and 1.0 g/kg for 27 January–28 February), $S_{ice}=0.5$ g/kg may appear to be a somewhat inconsistent choice. However, as mentioned in Section 3, although ice salinity in the northernmost parts of the Baltic Sea is generally lowest, ice salinity can be spatially quite variable and can change relatively rapidly with time.

- (4) Water salinity: Water salinity is assumed to be $S_{water}=3$ g/kg in the Bay of Bothnia and $S_{water}=5$ g/kg in the Sea of Bothnia (Janssen et al., 1999). For our model calculations we use a constant value of $S_{water}=4$ g/kg. Within this range (± 1 g/kg), the direct impact of the chosen water salinity value on the modelled brightness temperature is negligible (<0.1 K, Table 1), although the indirect impact via the changing freezing temperature of water, which is assumed to be the temperature of the underlying water, is somewhat higher (up to 2.7 K, Table 1).
- (5) Water temperature: As in Section 4, water is assumed to be at freezing temperature, that is, $T_{water}=-0.2^{\circ}\text{C}$ for the assumed water salinity.
- (6) Snow cover: As in Section 4, we estimate the snow thickness from eqs. (1) and (2). Again, snow is assumed to be dry, and we use the average snow density from model simulations in the Baltic Sea (Saloranta, 2000), which is $\rho_{snow}=325$ kg/m³ for March.

The main reasons why we use constant values for the above mentioned ice parameters in the emission model are: (1) Although we partly do have information on the ice parameters on a finer temporal and/or spatial resolution, neither do we have all auxiliary data sets simultaneously on a higher resolved scale, nor are the SMOS data available on a sub-daily basis, for example. (2) Individual SMOS measurements have a relatively high variability and information is more reliably extractable from spatially and temporally averaged SMOS data, which requires an appropriate averaging of the simulated brightness temperatures, too.

5.3. Results

First, we compare the ice thickness distributions as obtained from the EM measurements for the 12 circles with the ice thicknesses retrieved from SMOS brightness temperature intensity, which is the average between horizontally and vertically polarised brightness temperatures (Fig. 12). Overall, we consider 663731 individual EM measurements with a mean ice thickness of 91 ± 78 cm and a modal ice thickness of 39 cm. The 12 EM ice thickness

distributions have quite similar shapes. For most of the circles, more than two-thirds of the measured ice thicknesses take values between 0 and 1 m. The distributions have quite long, exponential tails representing ice thicknesses of up to 5 m or even more (e.g. in circles 9 and 10, but ice thicknesses $d_{ice} > 5$ m not depicted here).

For eight out of the 12 circles (circles 1–6, 11, 12), 69–85% of the measured ice thicknesses are below 1 m, and 13–21% of the ice thicknesses are between 1 and 2 m. In the three circles 7–9, still a majority of the ice thicknesses (54–69%) are below 1 m, and 25–29% are between 1 and 2 m. The highest ice thicknesses are found within circle 10, where only 39% of the ice has been measured to be less than 1 m thick. The second peak at about 1 m in the ice thickness distribution in circle 10 mainly originates from one flight section along the fast ice edge close to the Finnish coast west of Vaasa (approximately at 63.1°N and 21.6°E). Here the ice thickness may have been overestimated by the EM Bird due to shallow waters and potential freshwater layers underneath the fast ice (as indicated in Section 2.5).

Except for one circle, the SMOS-retrieved ice thicknesses are closer to the modal EM values than to the mean EM values (Fig. 12). In six out of the 12 circles, the SMOS and the EM modal ice thicknesses differ by one bin (6 cm) or less. In 10 out of the 12 circles, the difference is not more than two bins (12 cm). On average, the SMOS retrieval overestimates the EM modal value; the average SMOS ice thickness is $\langle d_{ice} \rangle = 49.0 \pm 8.1$ cm, while the average modal EM ice thickness is 41.0 ± 6.4 cm. The root mean square difference between the 12 EM modal and the 12 SMOS ice thicknesses is 11.5 cm and their coefficient of determination is $r^2=0.14$. The results for the SMOS retrieval are quite similar if we use only the horizontal ($\langle d_{ice} \rangle = 51.0 \pm 9.9$ cm, $r^2 = 0.18$) or only the vertical polarisation ($\langle d_{ice} \rangle = 48.0 \pm 4.9$ cm, $r^2 = 0.08$). While the retrieval that uses SMOS brightness temperature intensities gives the same range of ice thicknesses as found for the EM modal values (33–63 cm), the retrieval that uses only horizontal polarisation results in a slightly broader range (33–69 cm) and the retrieval that uses only vertical polarisation results in a narrower range (39–57 cm) of values.

In order to have a closer look at the observed brightness temperatures and the information they contain, we compare the SMOS observations with brightness temperatures that are simulated using the EM ice thickness distribution [eq. (3)], the modal EM ice thickness, or the mean EM ice thickness (Figs. 13 and 14). Regarding the incidence angle dependency, the observed and the simulated brightness temperatures appear to agree reasonably (Fig. 13). Though, the observed vertically polarised brightness temperatures at high incidence angles seem to deviate upwards compared to the simulated curves. This might be related to a higher land

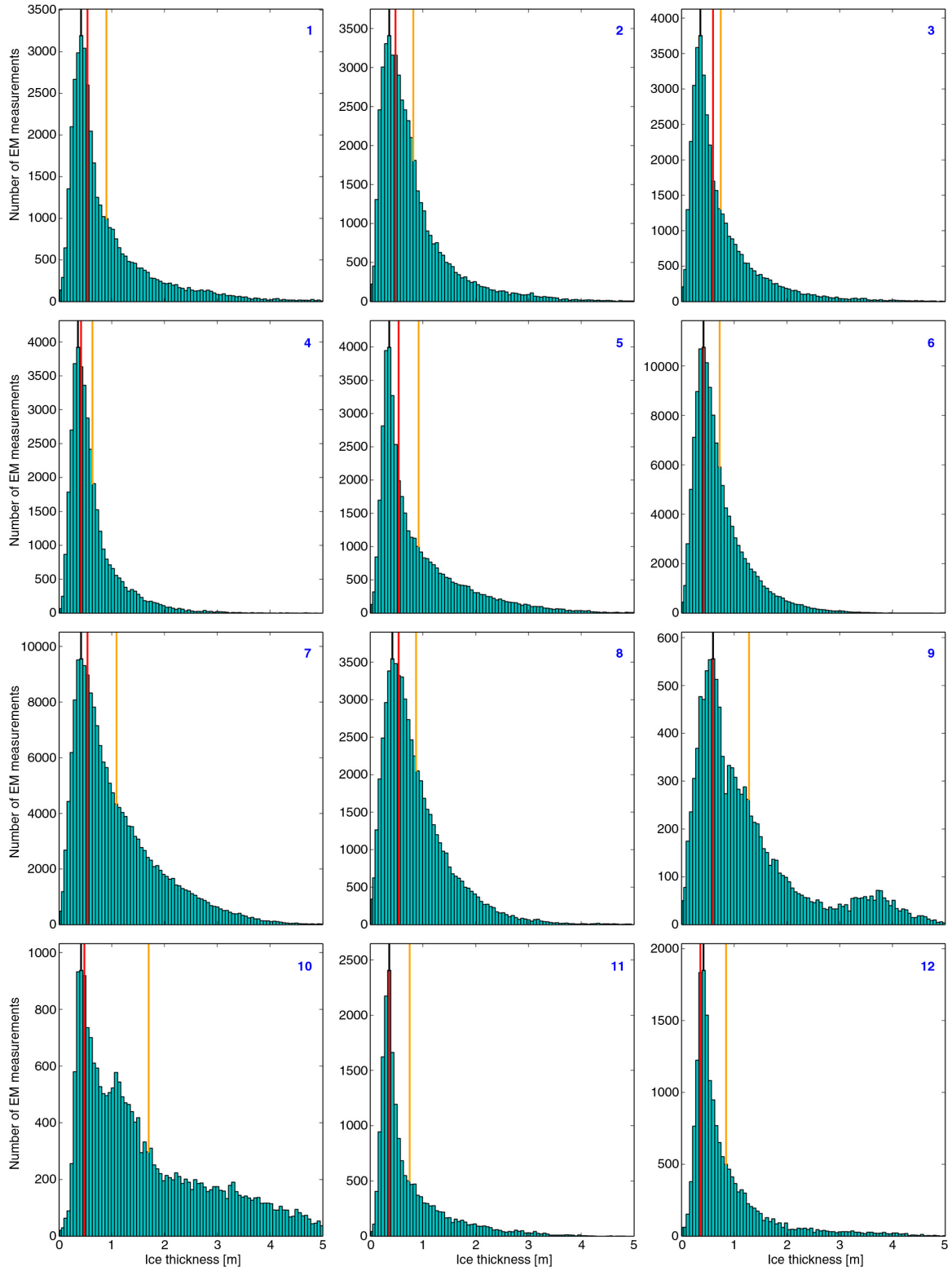


Fig. 12. Distribution of total EM ice thicknesses (i.e. sum of ice and snow thickness) within the circular areas depicted and numbered in Fig. 7. The red lines indicate total ice thickness as retrieved from SMOS brightness temperature intensities. The black lines indicate the modal values of the EM ice thickness distributions, while the orange lines indicate the EM mean ice thicknesses.

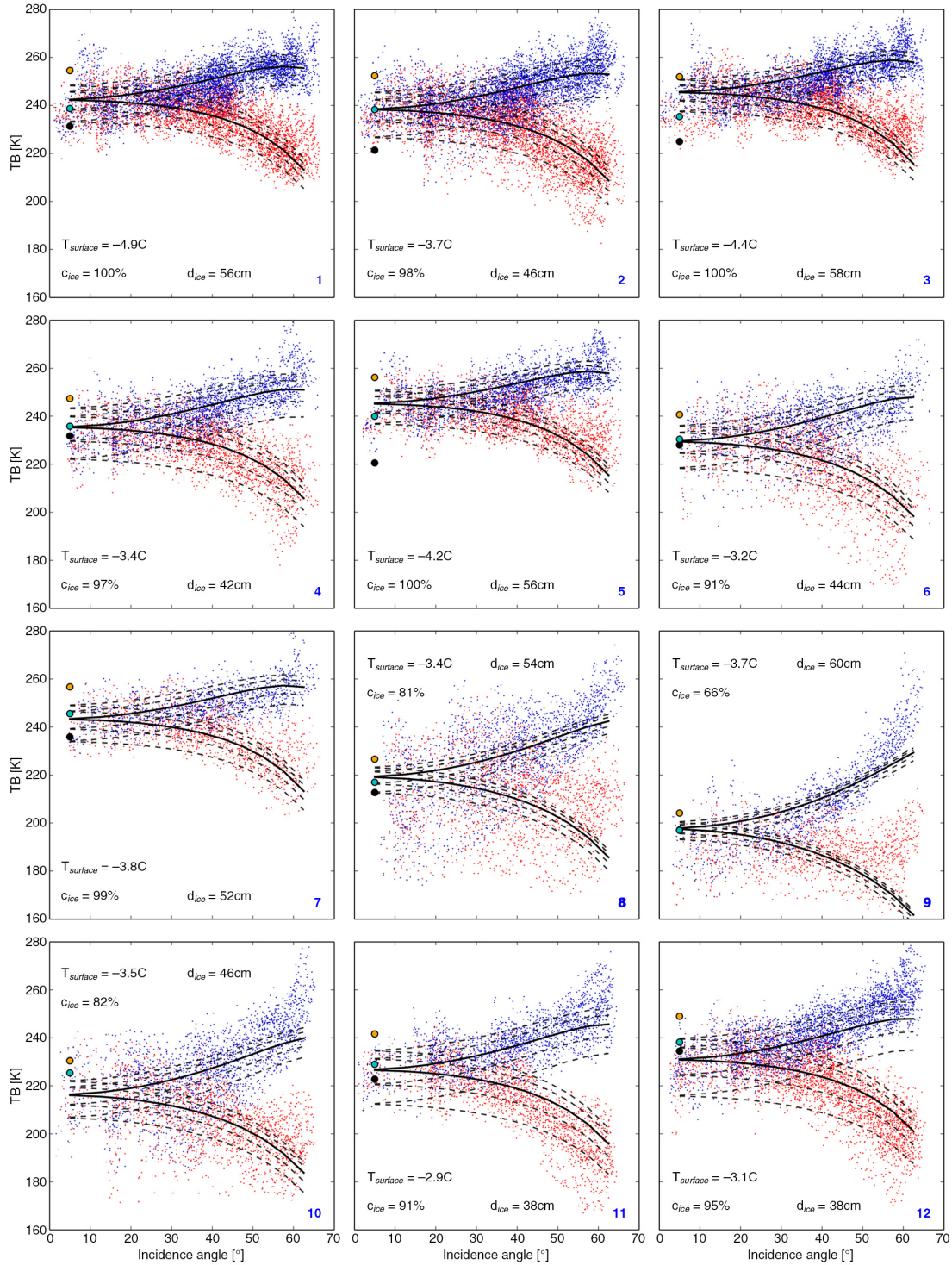


Fig. 13. SMOS brightness temperature (TB) versus incidence angle for the 12 circles. Blue dots indicate vertical, red dots horizontal polarisation. Solid black lines show the simulated brightness temperature curves with the lowest root mean square deviation from the SMOS observations. Dashed black lines show the simulated curves for the two higher and two lower ice thickness classes, respectively. Cyan circles indicate brightness temperature as simulated for the EM ice thickness distribution of the considered circle, while black circles indicate brightness temperature as simulated for the EM modal ice thickness and orange circles for the EM mean ice thickness. The mean surface temperature and the mean ice concentration as used in the simulations are given in the figures.

impact due to the larger footprints at higher incidence angles. The nadir ($\theta = 0^\circ$) brightness temperatures of the simulated Tb - θ -curves that describe the observations best (i.e. have the lowest root mean square deviations) and of the Tb - θ curves that are simulated using the EM ice thickness distributions show good agreement (Fig. 14). The coefficient of determination is $r^2 = 0.87$ and the mean deviation is less than 0.1 K. The nadir brightness temperatures simulated for the EM modal values have a higher deviation (6.6 K) and a considerably lower coefficient of determination ($r^2 = 0.45$). While the simulations that use the EM mean values are on average about 12 K higher than the nadir brightness temperatures of the observed curves, the simulations for the mean EM value result in the highest coefficient of determination ($r^2 = 0.95$).

Regarding the ice thickness, the two circles with the highest deviations (more than two ice thickness bins) between the SMOS retrieval and the modal EM ice thickness are circles 3 and 5 in the northern part of the campaign area along the coast (Fig. 15). Regarding the brightness temperature, the highest deviations (more than 6 K) between the simulations (for the EM ice thickness distributions) and the observations are found for circles 3, 10 and 12, for which possible explanations are discussed in Section 5.5. Thus, only for circle 3 both measures agree in that the deviation is especially high.

5.4. Sensitivity of brightness temperature to different ice parameters

As in Section 4.4, we now try to estimate and to compare the impact of the different model input parameters on our simulations and the resulting uncertainty for a potential SMOS ice thickness retrieval under the encountered ice conditions (Table 1). The largest difference to the analysis for January/ February 2011 in the previous section is that it was much warmer during the SafeWin campaign. At high ice temperatures, the model is very sensitive to ice temperature. The assumed uncertainty of 1 K for the averaged ice surface temperature is slightly lower than the uncertainty given in the MODIS product, which is 1.2–1.3 K (Hall et al., 2004). For the uncertainty of the ice salinity, we use the standard deviation of the measurements during the SafeWin campaign, that is, 0.1 g/kg. The ranges for the snow density, snow thickness, water salinity and water temperature are the same as for the ice in January/ February, partly with slightly different average values. For the ice concentration uncertainty, we use a smaller value (2%) than usually given for passive microwave ice concentration algorithms [e.g. 5% for ice concentrations higher than 90% (Andersen et al., 2007)], because we here used high-resolution optical MODIS data. As in Section 4.4, the ice thickness has the

highest impact on the brightness temperature as compared to the other ice parameters. The higher ice temperature and the lower ice salinity as compared to the January/February investigations come with both higher sensitivities to these parameters and lower sensitivity to the ice thickness. Under the ice conditions encountered during the SafeWin campaign in March 2011, the estimated uncertainty for the SMOS ice thickness retrieval is about 11 cm. Considering the challenging conditions in the Baltic Sea for the EM measurements, this value is similar to the uncertainty of the EM modal ice thickness.

5.5. Discussion

The highest deviations between the brightness temperature observations and simulations (for the EM ice thickness distributions) were found for circles 3, 10 and 12. The high deviations may be explained by the following findings: (1) Circles 10 and 12 are among the circles in that the number of EM measurements is notably lower (below about 22 000 measurements in circles 9–12) than in the remaining circles (more than 60 000 in circles 1–8), which could indicate that the ice thickness distributions obtained from the EM measurements are less representative. (2) Within circles 10 and 12, a small fraction of the EM measurements was carried out over fast ice, which we expected to result in an overestimation of ice thickness (Sections 2.5 and 5.3). Indeed, as expected for thicker ice the brightness temperatures simulated for the ice thickness distributions in circles 10 and 12 are higher than the observed brightness temperatures. (3) Additionally, circle 10 is one of the three circles in which the ice concentration during the campaign varied by more than 10% (Fig. 10). (4) The MODIS image from 6 March shows a lead in the ice within circle 12 that had not been visible in the MODIS image from 3 March (mentioned in Section 5.2). The EM measurements in circle 12 were carried out on 3 March (Fig. 2) when the lead had not yet opened up. Thus, we may hypothesise that after the lead opened the thicker ice close to the coast drifted off the coast, resulting in a lower average ice thickness on the following days. Consequently, the brightness temperature simulated for the ice thickness distribution on 3 March should be higher than the observed average brightness temperature during 2–7 March. Indeed, the simulations overestimate the SMOS observations in circle 12 (Figs. 13 and 14). (5) Among the 12 circles, circle 3 shows the highest variability of the ice surface temperature during the campaign with a surface temperature of more than -2°C on 4 March and less than -7°C on 5 March (Fig. 11). Thus, the simulations for circle 3 are more affected by potential non-linear temperature effects on the brightness temperature, which are not accounted for when we assume an average ice surface temperature in the emission model.

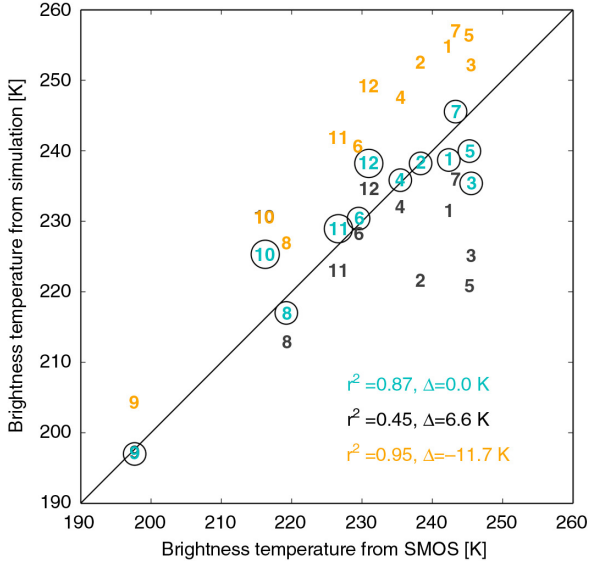


Fig. 14. Different brightness temperature simulations versus SMOS brightness temperature observations. The numbers indicate the circular areas. The colours correspond to the colours used for the circles in Fig. 13, that is, brightness temperatures simulated for the EM ice thickness distribution (cyan), for the modal EM ice thickness (black) and for the mean EM ice thickness (orange). The corresponding coefficients of determination and the mean deviations between the simulations and the observations are given in the figure.

The selection of the circular areas for the comparison of SMOS and EM data was done manually, the main goal being a representative coverage by EM measurements.

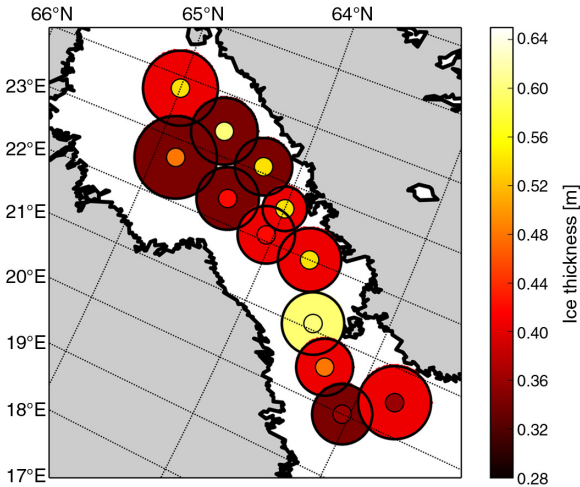


Fig. 15. Total ice thicknesses (i.e. sum of snow and ice thickness) as measured by the EM Bird and as retrieved from SMOS brightness temperature intensities. The inner circles depict ice thicknesses as retrieved from SMOS, the outer circles depict the modal values of all EM ice thicknesses measured within the corresponding circle.

This is, for example, reflected by the size of the circles, the circle with the highest spatial density of EM flights is the smallest, the more sparsely covered circles are larger. Additionally, the selection of the areas aimed for finding a reasonable compromise between a representative number of EM measurements and preferably constant ice conditions, as assumed within the emission model. This is also demonstrated by the average values and the temporal evolutions of the ice concentration and the ice surface temperature within the circles (Figs. 10 and 11). For example, the average ice concentrations of the 12 circles differ by up to 34%, while the variations within the circles are notably lower than 10% for most of the circles. Regarding the ice surface temperature, the values are generally lower in the northerly parts of the campaign area than in the southerly parts. However, this general North–South temperature gradient, as indicated in Fig. 11, is not directly reflected in the average values (given in Fig. 13), which is due to the missing ice surface temperature values for the northernmost circles at the first and the last days of the campaign.

In addition to the presented approach based on the 12 circular areas, we have performed a more commonly used grid approach for comparing the two data sets (not shown). We defined a regular grid with cell sizes of 30 km \times 30 km and collected all SMOS and EM data located within each grid cell. While the SMOS retrieval gave similar ice thicknesses as for the 12 circles, the EM modal ice thicknesses within the grid cells took values from a much broader range of ice thicknesses than found for the 12 circles. This is consistent with findings that profile lengths of at least 50 km (for relatively homogeneous ice) are necessary for the modal ice thickness to be a representative value for the observed ice thickness distribution (Rabenstein et al., 2010). Another reason why a grid-based comparison of EM and SMOS data is less suitable in this case is that here irregularly distributed field campaign data are compared with satellite data distributed on a regular grid and that the footprint sizes of the two data sets are very different. Thus, an alternative albeit manual approach appears to be more representative for the considered case.

In this study, we used an emission model based on the model by Burke et al. (1979). Because the Burke model neglects higher order reflection terms, we have compared our emission model with an emission model that accounts for these terms (Mills and Heygster, 2011), as has also been done in Maaß et al. (2013a). We found that for the ice conditions in Section 4, neglecting the higher order reflection terms leads to a difference in brightness temperature of 2–4 K at horizontal polarisation and differences below 1 K at vertical polarisation. For the ice conditions in Section 5, we found that brightness temperature intensities in the two models differed by about 1 K. Thus, we think that using an

emission model that accounts for higher order reflection terms would not change our results and would only have a minor impact on the retrieval of ice thickness in the Baltic Sea. However, for a future retrieval of ice thickness one may consider using a more accurate emission model for calculating brightness temperatures because the higher order reflection terms become more important for thinner ice layers. Another conceivable improvement of the model would be to replace the bulk ice permittivity in the model with a permittivity value that represents the permittivity profile within the ice or possibly the impact of the formation of snow-ice. An improved emission model could also contain the effects of ice roughness or an estimation of the uncertainty induced by ice roughness.

In the retrieval here, we used SMOS brightness temperatures at incidence angles θ ranging from 0 to 65°, while in previous studies (e.g. Kaleschke et al., 2012) the retrieval was based on brightness temperature intensities averaged over incidence angles between 0 and 40°. The advantage of including a broad range of incidence angles is that we can include more SMOS measurements, which, given the high variability of individual SMOS measurements, stabilises the retrieval. The disadvantage of including the higher incidence angle observations is the footprint size, which increases with increasing incidence angle. Thus, the measurements are blurred and may suffer more heavily from land spill-over. However, in our study, the results changed only slightly if we changed the incidence angle range. In Section 5.3, we obtained a coefficient of determination of $r^2 = 0.87$ and a mean deviation of $\Delta = 0.0$ K for the comparison of the nadir brightness temperatures of the $Tb-\theta$ curves obtained from SMOS observations and from our intensity simulations at $\theta = 0 \dots 65^\circ$ for the EM ice thickness distributions. If we, for example, used only $\theta = 0 \dots 40^\circ$ or $\theta = 20 \dots 30^\circ$ instead, r^2 increased to up to 0.93, while at the same time Δ increased to up to 1.3 K. Neither did we find substantial differences whether we used the brightness temperature intensity or only horizontal or vertical polarisation. For example, using only horizontal polarisation resulted in $r^2 = 0.82$ and $\Delta = 0.3$ K, while using only vertical polarisation gave $r^2 = 0.92$ and $\Delta = -0.7$ K. Thus, even if r^2 slightly increased by using a different range of incidence angles or a different polarisation, usually the mean deviation Δ increased simultaneously. Furthermore, for a comparison of only 12 values, the resulting differences are not significant, and based on the study here we are not able to give a recommendation as to which of the different options to use for a potential ice thickness retrieval in the future.

We expected the ice thickness from the SMOS retrieval to be rather interpretable as the modal than the mean ice thickness. First, because the modal value is considered to be the most accurate value obtained from EM measurements (Haas et al., 2010). Second, the maximum ice

thickness value that is retrievable from L-band brightness temperatures under Baltic conditions is up to 1.5 m (Kaleschke et al., 2010), and larger ice thicknesses have only a minor impact on the brightness temperature signal. Indeed, as the modal ice thicknesses of the EM distributions were notably smaller than the mean ice thicknesses, the brightness temperature simulations for the modal values had lower deviations from the observations than the simulations for the EM mean values. However, the correlation with the observations was much higher for the simulations that use the mean value ($r^2 = 0.95$) than for the ones that use the modal value ($r^2 = 0.45$). Although the L-band brightness temperature is only slightly dependent on how thick the thicker ice is, that is, the ice that is thicker than the maximum retrievable ice thickness, the fraction of thicker ice certainly has an impact on the brightness temperature. In this study, the mean ice thickness appears to contain more information on the fraction of thick ice within the considered area. Accordingly, the modal values show a higher variability among the 12 circles than the mean values because the 12 considered areas mainly differ in the higher ice thickness part of the thickness distribution. However, the highest agreement between observed and simulated brightness temperatures was found for the simulations that take into account the ice thickness distribution instead of using a single value. This finding has some implications for the interpretation of the ice thickness retrieved from SMOS data. The more we know about the shape of the thickness distribution for a considered time and area, the more meaningful is the information we can extract from the SMOS-retrieved ice thickness. Tian-Kunze et al. (2014) have started taking this effect into account by assuming that the ice thickness follows a lognormal distribution. Their SMOS retrieval then returns the mean value of such a distribution. However, while the statistical parameters for the lognormal distribution had been estimated from airborne ice thickness measurements mainly taken over thick multiyear ice, the SMOS retrieval itself was mainly performed over thinner first-year ice, which the SMOS retrieval is usually more suited for. Thus, this statistical retrieval approach requires further investigations.

6. Summary and conclusions

In this study, we considered L-band brightness temperatures at 1.4 GHz during the ice growth season in January and February 2011 in the Bay of Bothnia (Section 4). In this challenging region with (1) a high impact by the surrounding land, that is, potential land spill-over effects due to the large SMOS footprint size, and (2) a potentially high level of RFI contamination, we observed an increase of brightness temperature at horizontal and at vertical polarisation by more than 20 K, which was most likely

primarily caused by the sea ice thickness increasing from about 25 to 56 cm. Only if we included a snow layer in the emission model, the brightness temperatures simulated for realistic values of the remaining ice parameters (e.g. ice temperature and salinity) agreed reasonably with the observations. The mean deviations between the simulations and the observations over the SMOS incidence angle range ($\theta = 0 \dots 65^\circ$) were then below ± 3.5 K, and the root mean square deviations took values of 3–9 K. We stated that absolute ice thickness values are possibly difficult to retrieve exactly because of the lack of information on ice salinity and the high sensitivity of the retrieval to ice salinity under brackish conditions. In low-salinity regions, an alternative may be to use tie points for a SMOS ice thickness retrieval in order to avoid the dependency on the ice salinity assumption. Alternatively, if the ice thickness is known, the high sensitivity to ice salinity could be used to infer information on the ice salinity itself.

In Section 5, we manually selected 12 circular areas with sizes on the order of the SMOS footprint (diameters of 36–66 km). We simulated brightness temperatures using 6-day mean values of ice concentration and of ice surface temperature, both obtained from MODIS, and of the ice thickness distribution obtained from EM measurements during the SafeWin campaign (2–7 March 2011). In contrast to previous studies, we did not assume a 100% ice coverage, but considered ice concentrations between 66 and 100%. The comparison of simulated and SMOS-observed brightness temperature intensity, that is, the average between horizontally and vertically polarised brightness temperatures, resulted in a coefficient of determination of $r^2 = 0.87$ and a mean deviation of less than 0.1 K. While r^2 was similarly high if we used the mean ice thickness in the simulations ($r^2 = 0.95$), the observed brightness temperatures were then overestimated by almost 12 K, here corresponding to a 8 cm difference between the EM mean and the SMOS-retrieved ice thicknesses. Compared to the simulations for the mean ice thickness, r^2 and the mean deviation decreased to about half of their values if the modal EM ice thickness was used. The results suggest: First, the SMOS ice thickness is closer to the modal than to the mean value of the EM ice thickness distribution, which is consistent with earlier findings that EM measurements are most suitable with respect to their modal value and with the measurement principle of SMOS, which implicates a maximum distinguishable ice thickness and a higher sensitivity to thinner ice. Second, in this study the variability of the SMOS brightness temperatures was more reasonably explained by the mean than the modal EM ice thickness. Third, the interpretation of SMOS-retrieved ice thickness ideally requires some knowledge on the shape of the ice thickness distribution. Finally, in principle, the currently used emission model appears to be able to capture the ice

thickness information contained in SMOS data, suggesting the retrieval's applicability also to regions other than the Baltic Sea.

7. Acknowledgements

The authors would like to thank the members of the ESA SMOSIce project for helpful discussions. This work was partly supported by the International Max Planck Research School on Earth System Modelling and in parts through the Cluster of Excellence 'CliSAP' (EXC177), University of Hamburg, funded through the German Science Foundation (DFG). SMOS data were provided by the ESA Support to Science Element programme under contract 4000101476. The Baltic EM thickness campaign and analysis was conducted within the EU-funded project 'Safety of winter navigation in dynamic ice' (contract SCP8-GA-2009-233884 – SAFEWIN). The partners in this project are Aalto University, Arctic and Antarctic Research Institute, Finnish Meteorological Institute, Finnish Transport Agency, ILS Oy, Stena Rederi AB, Swedish Maritime Administration, Swedish Meteorological and Hydrological Institute, Tallinn University of Technology and AS Tallink Group. Finally, we are grateful to three anonymous reviewers for their helpful and considerate comments.

References

- Alexandrov, V., Sandven, S., Wahlin, J. and Johannessen, O. 2010. The relation between sea ice thickness and freeboard in the arctic. *Cryosphere*. **4**(3), 373–380. DOI: 10.5194/tc-4-373-2010.
- Andersen, S., Tonboe, R., Kaleschke, L., Heygster, G. and Pedersen, L. 2007. Intercomparison of passive microwave sea ice concentration retrievals over the high-concentration Arctic sea ice. *J. Geophys. Res.* **112**(C8), C08.
- Barber, D. G., Fung, A., Grenfell, T. C., Nghiem, S. V., Onstott, R. G. and co-authors. 1998. The role of snow on microwave emission and scattering over first-year sea ice. *IEEE Trans. Geosci. Remote Sens.* **36**(5), 1750–1763.
- Burke, W., Schmugge, T. and Paris, J. 1979. Comparison of 2.8- and 21-cm microwave radiometer observations over soils with emission model calculations. *J. Geophys. Res.* **84**(C1), 287–294. DOI: 10.1029/JC084iC01p00287.
- Cox, G. and Weeks, W. 1983. Equations for determining the gas and brine volumes in sea ice samples. *J. Glaciol.* **29**(102), 306–316.
- Doane, D. P. 1979. Aesthetic frequency classifications. *Am. Stat.* **30**(4), 181–183.
- CESBIO, Expert Support Laboratories IPSL-Service d'Aéronomie, INRA-EPHYSE, Reading University, Tor Vergata University. 2007. *SMOS Level 2 Processor for Soil Moisture – Algorithm Theoretical Based Document (ATBD)*. Array Systems Computing Inc., Toronto, Canada.
- Fofonoff, N. and Millard, R. 1983. *Algorithms for Computation of Fundamental Properties of Seawater*. Technical Report 44, UNESCO, Technical Papers in Marine Science, Paris, France.

- Frey, R., Ackerman, S. A., Liu, Y., Strabala, K., Zhang, H. and co-authors. 2008. Cloud detection with MODIS. Part I: Improvements in the MODIS cloud mask for collection 5. *J. Atmos. Ocean. Technol.* **25**, 1057–1072.
- Granskog, M., Kaartokallio, H., Kuosa, H., Thomas, D. and Vainio, J. 2006. Sea ice in the Baltic Sea—a review. *Estuar. Coast Shelf Sci.* **70**(1–2), 145–160.
- Haas, C. 2006. Airborne electromagnetic sea ice thickness sounding in shallow, brackish water environments of the Caspian and Baltic Seas. In: *Proceedings of OMAE2006 25th International Conference on Offshore Mechanics and Arctic Engineering*, ASME (American Society of Mechanical Engineers), Hamburg, Germany, 6.
- Haas, C. and Casey, A. 2012. *Helicopterborne EM Ice Thickness Surveys During SafeWin 2011 Field Campaign*. Technical Report, University of Alberta, Edmonton, Canada.
- Haas, C., Hendricks, S., Eicken, H. and Herber, A. 2010. Synoptic airborne thickness surveys reveal state of Arctic sea ice cover. *Geophys. Res. Lett.* **37**(9), L09501.
- Haas, C. and Jochmann, P. 2003. Continuous EM and ULS thickness profiling in support of ice force measurements. In: *Proceedings of the 17th International Conference on Port and Ocean Engineering under Arctic Conditions, POAC 03* (eds. S. Loeset, B. Bonnemaire and M. Bjerkas). Department of Civil and Transport Engineering, Norwegian University of Science, Trondheim, Norway, pp. 849–856.
- Haas, C., Lobach, J., Hendricks, S., Rabenstein, L. and Pfaffling, A. 2009. Helicopter-borne measurements of sea ice thickness, using a small and lightweight, digital EM system. *J. Appl. Geophys.* **67**(3), 234–241.
- Hall, D., Key, J., Casey, K., Riggs, G. and Cavalieri, D. 2004. Sea ice surface temperature product from MODIS. *IEEE Trans. Geosci. Remote Sens.* **42**(5), 1076–1087. DOI: 10.1109/TGRS.2004.825587.
- Hallikainen, M. 1992. Chapter: Microwave remote sensing of low-salinity sea ice. *Microwave Remote Sensing of Sea Ice*, (ed. F.D. Carsey), AGU, Washington, DC, pp. 361–373.
- Huntemann, M., Heygster, G., Kaleschke, L., Krumpen, T., Mäkynen, M. and co-authors. 2014. Empirical sea ice thickness retrieval during the freeze up period from SMOS high incident angle observations. *Cryosphere*. **8**(2), 439–451. DOI: 10.5194/tc-8-439-2014.
- Hwang, B. J., Ehn, J. K., Barber, D. G., Galley, R. and Grenfell, T. C. 2007. Investigations of newly formed sea ice in the Cape Bathurst polynya: 2. Microwave emission. *J. Geophys. Res.* **112**(C5), C05003.
- Janssen, F., Schrum, C. and Backhaus, J. 1999. A climatological data set of temperature and salinity for the Baltic Sea and the North Sea. *Deutsche Hydrographische Zeitschrift*. **51**, 5–245.
- Kaleschke, L., Lüpkes, C., Vihma, T., Haarpaintner, J., Bochert, A. and co-authors. 2001. SSM/I sea ice remote sensing for mesoscale ocean-atmosphere interaction analysis. *Can. J. Remote Sens.* **27**(5), 526–537.
- Kaleschke, L., Maaß, N., Haas, C., Hendricks, S., Heygster, G. and co-authors. 2010. A sea-ice thickness retrieval model for 1.4 GHz radiometry and application to airborne measurements over low salinity sea-ice. *Cryosphere*. **4**, 583–592. DOI: 10.5194/tc-4-583-2010.
- Kaleschke, L., Tian-Kunze, X., Maaß, N., Mäkynen, M. and Drusch, M. 2012. Sea ice thickness retrieval from SMOS brightness temperatures during the Arctic freeze-up period. *Geophys. Res. Lett.* **39**, L05501. DOI: 10.129/2012GL050916.
- Kawamura, T., Shirasawa, K., Ishikawa, N., Lindfors, A., Rasmus, K. and co-authors. 2001. Time-series observations of the structure and properties of brackish ice in the Gulf of Finland. *Ann. Glaciol.* **33**(1), 1–4.
- Kerr, Y., Waldteufel, P., Wigneron, J., Martinuzzi, J., Font, J. and co-authors. 2001. Soil moisture retrieval from space: the Soil Moisture and Ocean Salinity (SMOS) mission. *IEEE Trans. Geosci. Remote Sens.* **39**(8), 1729–1735.
- Klein, L. and Swift, C. 1977. An improved model for the dielectric constant of sea water at microwave frequencies. *IEEE Trans. Antennas Propag.* **25**(1), 104–111. DOI: 10.1109/TAP.1977.1141539.
- Kwok, R. and Rothrock, D. 2009. Decline in Arctic sea ice thickness from submarine and ICESat records: 1958–2008. *Geophys. Res. Lett.* **36**(15), L15501.
- Laxon, S., Peacock, N. and Smith, D. 2003. High interannual variability of sea ice thickness in the Arctic region. *Nature*. **425**(6961), 947–950.
- Leppäranta, M. and Hakala, R. 1992. The structure and strength of first-year ice ridges in the Baltic Sea. *Cold Reg. Sci. Technol.* **20**(3), 295–311.
- Leppäranta, M. and Myrberg, K. 2009. *Physical Oceanography of the Baltic Sea*. Springer Science & Business Media, Chichester, UK.
- Maaß, N. 2013. Remote sensing of sea ice thickness using SMOS data. *Reports on Earth System Science* 131. Online at: http://www.mpimet.mpg.de/fileadmin/publikationen/Reports/WEB_BzE_131.pdf
- Maaß, N. and Kaleschke, L. 2010. Improving passive microwave sea ice concentration algorithms for coastal areas: applications to the Baltic Sea. *Tellus A*. **62**(4), 393–410. DOI: 10.1111/j.1600-0870.2010.00452.x.
- Maaß, N., Kaleschke, L., Tian-Kunze, X. and Drusch, M. 2013a. Interactive comment on Snow thickness retrieval over thick Arctic sea ice using SMOS satellite data by N. Maaß et al. *Cryosphere Discuss.* **7**, C1480–C1484.
- Maaß, N., Kaleschke, L., Tian-Kunze, X. and Drusch, M. 2013b. Snow thickness retrieval over thick Arctic sea ice using SMOS satellite data. *Cryosphere*. **7**(6), 1971–1989. DOI: 10.5194/tc-7-1971-2013.
- Maaß, N., Kaleschke, L., Tian-Kunze, X. and Tonboe, R. T. 2015. Snow thickness retrieval from L–band brightness temperatures: a model comparison. *Ann. Glaciol.* **56**(69), 9–17.
- Mäkynen, M. 2012. SMOSIce-DAT user manual for the validation data. *STSE-SMOS Sea Ice Retrieval Study SMOSIce Final Report*, (ed. L. Kaleschke), European Space Agency, Hamburg, Germany, pp. 285–346.
- Mäkynen, M., Cheng, B. and Similä, M. 2013. On the accuracy of thin-ice thickness retrieval using MODIS thermal imagery over Arctic first-year ice. *Ann. Glaciol.* **54**(62), 87.

- Martin, S., Drucker, R., Kwok, R. and Holt, B. 2004. Estimation of the thin ice thickness and heat flux for the Chukchi Sea Alaskan coast polynya from Special Sensor Microwave/Imager data, 1990–2001. *J. Geophys. Res.* **109**, C10012. DOI: 10.1029/2004JC002428.
- Mecklenburg, S., Drusch, M., Kerr, Y., Font, J., Martin-Neira, M. and co-authors. 2012. ESA's soil moisture and ocean salinity mission: mission performance and operations. *IEEE Trans. Geosci. Remote Sens.* **50**(5), 1354–1366. DOI: 10.1109/TGRS.2012.2187666.
- Mills, P. and Heygster, G. 2011. Sea ice emissivity modeling at L-band and application to 2007 Pol-Ice campaign field data. *IEEE Trans. Geosci. Remote Sens.* **49**(2), 612–627.
- Naoki, K., Ukita, J., Nishio, F., Nakayama, M., Comiso, J. C. and co-authors. 2008. Thin sea ice thickness as inferred from passive microwave and in situ observations. *J. Geophys. Res.* **113**(C2), C02S16.
- Nihashi, S., Ohshima, K. I., Tamura, T., Fukamachi, Y. and Saitoh, S.-I. 2009. Thickness and production of sea ice in the Okhotsk Sea coastal polynyas from AMSR-E. *J. Geophys. Res. Oceans (1978–2012)*. **114**(C10), C10025.
- Oliva, R., Daganzo, E., Kerr, Y., Mecklenburg, S., Nieto, S. and co-authors. 2012. SMOS radio frequency interference scenario: status and actions taken to improve the RFI environment in the 1400–1427-MHz passive band. *IEEE Trans. Geosci. Remote Sens.* **50**(5), 1427–1439.
- Palosuo, E. 1961. Crystal structure of brackish and freshwater ice. *Int. Assoc. Hydrol. Sci. Snow Ice Comm.* **54**, 9–14.
- Palosuo, E. 1963. The Gulf of Bothnia in winter. II. Freezing and ice forms. *Merentutkimuslaitoksen julkaisu/Havsforskningsinstitutets skrift*. **209**, 1–64.
- Palosuo, E., Leppäranta, M. and Seinä, A. 1982. Formation, thickness and stability of fast ice along the Finnish coast. *Styrelsen för Vintersjöfartforskning/Winter Navigation Research Board*. **36**, 51.
- Perovich, D. K., Longacre, J., Barber, D. G., Maffione, R. A., Cota, G. F. and co-authors. 1998. Field observations of the electromagnetic properties of first-year sea ice. *IEEE Trans. Geosci. Remote Sens.* **36**(5), 1705–1715.
- Pinori, S., Crapolicchio, R. and Mecklenburg, S. 2008. Preparing the ESA-SMOS (soil moisture and ocean salinity) mission-overview of the user data products and data distribution strategy. In: *Microwave Radiometry and Remote Sensing of the Environment, MICRORAD*, IEEE, Firenze, Italy, pp. 1–4.
- Pounder, E. 1965. *The Physics of Ice*. Oxford, Pergamon Press. The Commonwealth and International Library, Geophysics Division. DOI: 10.1119/1.1973537.
- Rabenstein, L., Hendricks, S., Martin, T., Pfaffhuber, A. and Haas, C. 2010. Thickness and surface-properties of different sea-ice regimes within the Arctic Trans Polar Drift: data from summers 2001, 2004 and 2007. *J. Geophys. Res.* **115**(C12), C12059.
- Saloranta, T. 2000. Modeling the evolution of snow, snow ice and ice in the Baltic Sea. *Tellus A*. **52**(1), 93–108.
- Spren, G., Kaleschke, L. and Heygster, G. 2008. Sea ice remote sensing using AMSR-E 89 GHz channels. *J. Geophys. Res.* **113**, C02S03.
- Tamura, T. and Ohshima, K. 2011. Mapping of sea ice production in the Arctic coastal polynyas. *J. Geophys. Res.* **116**(C7), C07030.
- Tian-Kunze, X., Kaleschke, L., Maaß, N., Mäkynen, M., Serra, N. and co-authors. 2014. SMOS derived sea ice thickness: algorithm baseline, product specifications and initial verification. *Cryosphere*. **8**(3), 997–1018.
- Tiuri, M., Sihvola, A., Nyfors, E. and Hallikainen, M. 1984. The complex dielectric constant of snow at microwave frequencies. *IEEE J. Ocean. Eng.* **9**(5), 377–382. DOI: 10.1109/JOE.1984.1145645.
- Vant, M., Ramseier, R. and Makios, V. 1978. The complex-dielectric constant of sea ice at frequencies in the range 0.1–40 GHz. *J. Appl. Phys.* **49**(3), 1264–1280. DOI: 10.1063/1.325018.
- Wessel, P. and Smith, W. 1996. A global, self-consistent, hierarchical, high-resolution shoreline database. *J. Geophys. Res. – Solid Earth*. **101**(B4), 8741–8743.
- Yu, Y. and Rothrock, D. 1996. Thin ice thickness from satellite thermal imagery. *J. Geophys. Res.* **101**(C11), 25753–25766.